Published in Chemistry of Materials 14, issue 3, pp. 1075–1090, 2012,
which should be used for any reference to this work

Aromatic Bent-Core Liquid Crystals: an Opportunity for Introducing Terdentate Binding Units into Mesophases

Homayoun Nozary,[†] Claude Piguet,*[,†] Jean-Pierre Rivera,[†] Paul Tissot,[†] Pierre-Yves Morgantini,[∞] Jacques Weber,[∞] Gérald Bernardinelli,[§] Jean-Claude G. Bünzli,[‡] Robert Deschenaux,[⊥] Bertrand Donnio,[#] Daniel Guillon[#]

Department of Inorganic, Analytical and Applied Chemistry, Department of Physical Chemistry, and Laboratory of X-ray Crystallography, University of Geneva, CH-1211 Geneva 4, Switzerland, Institute of Molecular and Biological Chemistry, Swiss Federal Institute of Technology, CH-1015 Lausanne, Switzerland, Institute of Chemistry, University of Neucha^tel, CH-2000 Neucha^tel, Switzerland, and Institute of Physics and Chemistry of Materials, F-67037 Strasbourg, France

Lipophilic linear semirigid side arms containing two or three successive phenyl rings separated by carboxylate spacers have been connected to the 5 or 6 positions of bent aromatic terdentate 2,6-bis(benzimidazol-2-yl)pyridine binding units to give extended V-shaped (**L11**) and I-shaped receptors (**L12**, **L12b**, and **L13**). The carboxylate spacers limit the flexibility of the side arms and provide crossed arrangements of the successive aromatic rings in the crystal structure of **L12b** ($C_{63}H_{61}N_5O_{10}$; triclinic, $P\bar{1}$, $Z = 2$) in agreement with semiempirical calculations performed on optimized gas-phase geometries. Moreover, the carboxylate spacers in **L11**−**L13** prevent efficient electronic delocalization between the connected aromatic rings and act as weak π acceptors producing a slight increase of the energy of the $^1\pi\pi^*$ and $^3\pi\pi^*$ levels centered on the terdentate binding unit. Intermolecular π-stacking interactions observed in the crystal of **L12b** are invoked to rationalize (i) the peculiar excimer emission of **L11** in the solid state and (ii) the rich and varied calamitic (I-shaped **L12**, **L12b**, and **L13**) and columnar (V-shaped **L11**) mesomorphism observed at high temperature. The Col_R mesophase detected for **L11** demonstrates that V-shaped bent terdentate binding units are compatible with liquid-crystalline behavior. Complexation of **L11** with lanthanide(III) produces I-shaped complexes [Ln(**L11**)$(NO_3)_3$] (Ln = La, Eu, Gd, Tb, and Lu) possessing a large axial anisometry as found in the crystal structure of [Lu(**L11**)$(CF_3CO_2)_3(H_2O)$] ($LuC_{81}H_{87}N_5O_{17}F_9$; triclinic, $P\bar{1}$, $Z = 2$), which exists in the solid state as H-bonded dimers. No mesomorphism is detected for the complexes as a result of the large perpendicular expansion brought by the metallic coordination site, but the high energy of the ligand-centered $^3\pi\pi^*$ prevents Eu($^5D_0$) → **L11** back transfer in the Eu(III) complex, which thus exhibits sizable red luminescence at room temperature, a crucial point for the design of luminescent materials.

Introduction

Chelating terdentate binding units are universally used as receptors for complexing d-block or f-block metal ions, and derivatives of the bent semirigid aromatic 2,2′;6′,2″-terpyridine (**L1**, Chart 1) have found numerous applications in coordination[1] and metallosupramolecular chemistry.[2,3] However, little interest has been focused on their use to develop metal-containing liquid crystals (metallomesogens) by taking advantage of the fascinating optical and magnetic properties of the metal ions to generate materials with enhanced physicochemical properties.[4] The major drawback concerns the aromatic bent core of the terpyridine unit, which does not match

* To whom correspondence should be addressed. E-mail: Claude.Piguet@chiam.unige.ch.
[†] Department of Inorganic, Analytical and Applied Chemistry, University of Geneva.
[∞] Department of Physical Chemistry, University of Geneva.
[§] Laboratory of X-ray Crystallography, University of Geneva.
[‡] Swiss Federal Institute of Technology.
[⊥] University of Neuchâtel.
[#] Institute of Physics and Chemistry of Materials, Strasbourg.

(1) (a) Constable, E. C. *Adv. Inorg. Chem. Radiochem.* **1986**, *30*, 69. (b) Cargill Thompson, A. M. W. *Coord. Chem. Rev.* **1997**, *160*, 1 and references therein.

(2) Lindoy, L. F.; Atkinson, I. M. *Self-Assembly in Supramolecular Systems*; The Royal Society of Chemistry: London, 2000; Chapters 3−6 and references therein.

(3) (a) Alcock, N. W.; Barker, P. R.; Haider, J. M.; Hannon, M. J.; Painting, C. L.; Pikramenou, Z.; Plummer, E. A.; Rissanen, K.; Saarenketo, P. *J. Chem. Soc., Dalton Trans.* **2000**, 1447. (b) Cardenas, D. J.; Collin, J.-P.; Gavina, P.; Sauvage, J.-P.; DeCian, A.; Fischer, J.; Armaroli, N.; Flamigni, L.; Vicinelli, V.; Balzani, V. *J. Am. Chem. Soc.* **1999**, *121*, 5481. (c) Takalo, H.; Mukkala, V.-M.; Meriö, L.; Rodriguez-Ubis, J. C.; Sedano, R.; Juanes, O.; Brunet, E. *Helv. Chim. Acta* **1997**, *80*, 372. (d) Mürner, H.-R.; Chassat, E.; Thummel, R. P.; Bünzli, J.-C. G. *J. Chem. Soc., Dalton Trans.* **2000**, 2809.

(4) (a) Ziessel, R.; Douce, L.; El-ghayoury, A.; Harriman, A.; Skoulios, A. *Angew. Chem., Int. Ed.* **2000**, *39*, 1489. (b) Tschierske, C. *Angew. Chem., Int. Ed.* **2000**, *39*, 2454.

Chart 1

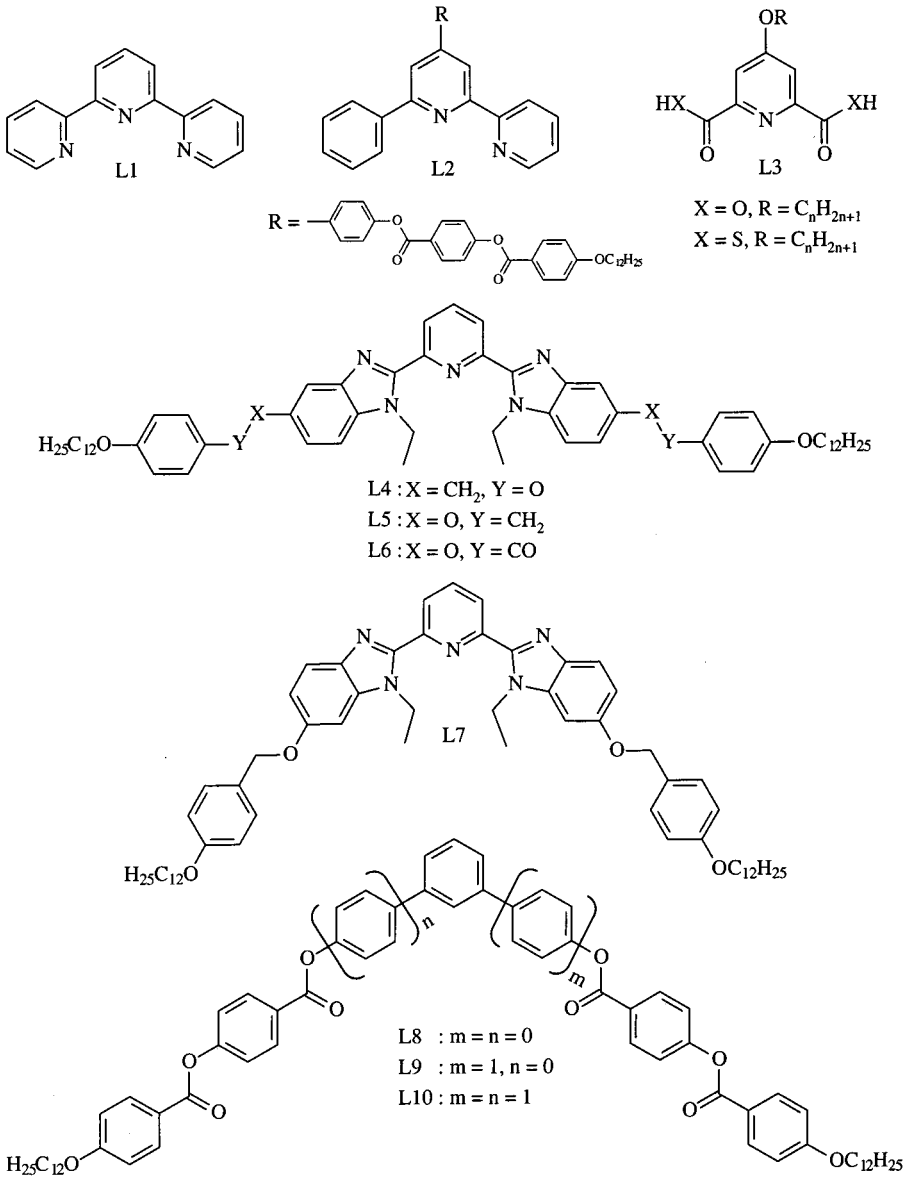

the molecular geometrical criteria required for calamitic (rodlike) or discotic (disklike) mesomorphism.[5] The first strategy developed to overcome this limitation uses the connection of semirigid lipophilic residues at the 4 position of the central pyridine ring in 6′-phenyl-2,2′-bipyridine (**L2**)[6] and pyridine-2,6-dithiocarboxylic acid (**L3**).[7] The resulting large perpendicular molecular anisometries are compatible with calamitic (nematic and smectic)[6] and columnar[7] mesomorphisms, which are observed for **L2** and for the Pd(II) tabular complexes of **L2** and **L3**. The alternative strategy connects semirigid lipophilic side arms at the 5 position of bent 2,6-bis(1-ethylbenzimidazol-2-yl)pyridine cores to give the extended receptors **L4**−**L6** (length/width ratio ≈ 10), which exhibit smectic and nematic mesomorphisms.[8] The connection of related side arms at the 6 position in **L7** provides a global V-shaped arrangement of the receptor associated with a limited anisometry (length/width ratio ≈ 1.2) and no mesomorphism.[9] Obvious geometrical criteria based on minimal axial anisotropies[5,10] have been invoked for rationalizing this drastic change,[9] but a deep understanding of the relationships between molecular anisometry of bent-core receptors and the mesomorphism of the associated materials is crucial for the design of lanthanide-containing metallomesogens because the complexation processes interconvert I- and V-shaped arrangements of the ligands (Figure 1).

(5) (a) *Metallomesogens, Synthesis, Properties and Applications*; Serrano, J. L., Ed.; VCH: Weinheim, Germany, 1996. (b) Donnio, B.; Bruce, D. W. *Struct. Bonding* **1999**, *95*, 193.

(6) (a) Neve, F.; Ghedini, M.; Crispini, A. *Chem. Commun.* **1996**, 2463. (b) Neve, F.; Ghedini, M.; Francescangeli, O.; Campagna, S. *Liq. Cryst.* **1998**, *24*, 673.

(7) Espinet, P.; Garcia-Orodea, E.; Miguel, J. A. *Inorg. Chem.* **2000**, *39*, 3645 and references therein.

(8) Nozary, H.; Piguet, C.; Tissot, P.; Bernardinelli, G.; Bünzli, J.-C. G.; Deschenaux, R.; Guillon, D. *J. Am. Chem. Soc.* **1998**, *120*, 12274.

(9) Nozary, H.; Piguet, C.; Rivera, J.-P.; Tissot, P.; Bernardinelli, G.; Vulliermet, N.; Weber, J.; Bünzli, J.-C. G. *Inorg. Chem.* **2000**, *39*, 5286.

(10) Toyne, K. J. *Critical Reports on Applied Chemistry*; Gray, G. W., Ed.; John Wiley & Sons: New York, 1987; Vol. 22, Chapter 2, p 28.

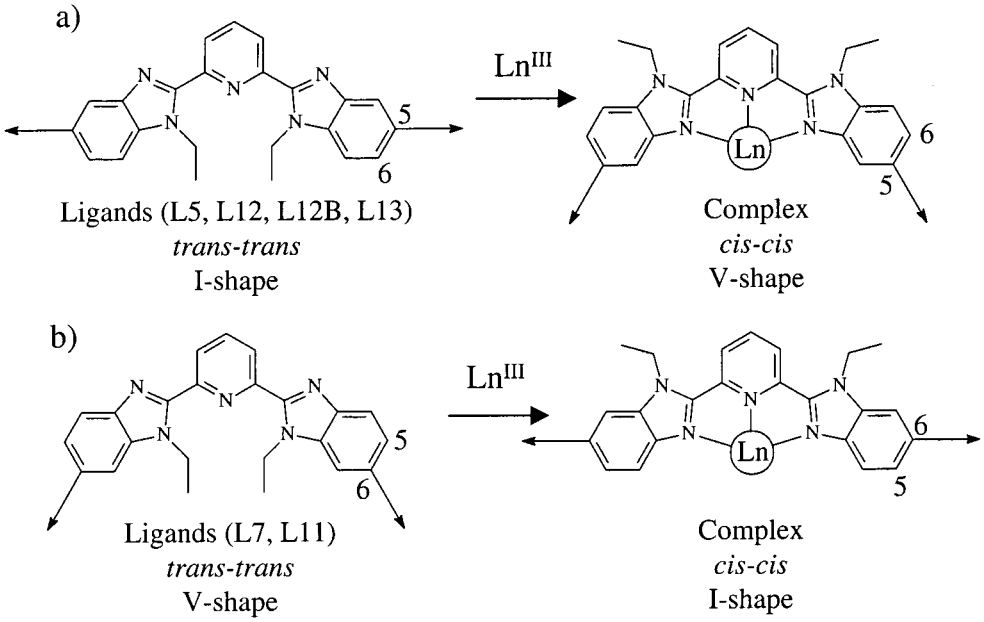

Figure 1. Conformational changes (trans−trans → cis−cis) occurring upon complexation to Ln(III) and associated schematic molecular anisometry observed for (a) five-substituted receptors (**L5**, **L12**, **L12B**, and **L13**) and (b) six-substituted receptors (**L7** and **L11**).

For uncoordinated ligands, the trans−trans conformation of the terdentate bis(benzimidazolyl)pyridine binding unit (i.e., the unsubstituted nitrogen atoms of the benzimidazole rings and that of the pyridine ring lie in trans arrangements) provides I-shaped (Figure 1a) and V-shaped (Figure 1b) receptors depending respectively on the extension along the 5 or 6 positions of the benzimidazole rings.[9] The trans−trans → cis−cis conformational change occurring upon complexation to the lanthanide metal ions [Ln(III)] transforms I-shaped arrangements into V-shaped arrangements and vice versa (Figure 1). Receptors **L5** (I-shaped)[8] and **L7** (V-shaped)[9] have been previously developed for a preliminar exploration of the influence of this conformational change on the liquid-crystalline and photophysical properties of the ligands and their lanthanide complexes, but the lack of mesomorphism observed for **L7** and for the complexes [Ln(**L*i***)$(NO_3)_3$] (*i* = **5** and **7**) led to the conclusions that (i) V-shaped arrangements of these receptors were not compatible with the formation of mesophases and (ii) lanthanide complexation drastically compromised liquid-crystalline behaviors in the resulting materials. However, Niori and co-workers reported in 1996 on smectic phases formed by banana-shaped Schiff-base derivatives,[11] and the occurrence of spontaneous symmetry breaking compatible with ferroelectric properties in these materials attracted great interest.[12,13] The recent design by Tschierske and co-workers[14] of banana-shaped molecules **L8** and **L9** producing antiferroelectric smectic C phases and the observation that the extended bent-core analogue **L10** gives a rectangular columnar Col_R phase at 165 °C[14] led us to reconsider the geometrical criteria limiting the formation of mesophases for the bent-core ligands **L4**−**L7**. In this paper, we demonstrate that the combination of semirigid polar carboxylate spacers with a minimum of two extra appended phenyl groups connected to the bent terdentate bis(benzimidazolyl)pyridine core induces calamitic mesomorphism for the extended I-shaped receptors **L*i*** (*i* = **5**, **12**, **12b**, and **13**, **5** substitution) and columnar mesomorphism for the related but V-shaped receptor **L11** (6 substitution, Chart 2). Particular attention has been focused on the structural and geometrical characteristics required for the formation of the mesophases together with their consequences on the electronic and photophysical properties of these materials. Theoretical calculations performed on optimized gas-phase geometries compared with solution- and solid-state structures give an insight into the intra- and intermolecular interactions responsible for the observed behavior. Complexation of **L11** with LnX_3 (X = NO_3^- and $CF_3CO_2^-$) to give [Ln(**L11**)$(NO_3)_3$] and [Ln(**L11**)$(CF_3CO_2)_3(H_2O)$] has been attempted to explore the potentiality of these extended receptors for producing new luminescent materials.

Results and Discussion

Synthesis of Ligands L11−L13. According to the convergent strategies developed for the syntheses of **L4**−**L7**, polyaromatic side arms bearing carboxylate spacers (Scheme 1) have been connected to the synthons **7** and **8** (Scheme 2).[8,9,15] ^1H NMR spectra in $CDCl_3$ display C_{2v}-symmetrical molecules compatible with an average planar structure on the NMR time scale. The systematic lack of nuclear Overhauser effects (NOEs) between the protons of the ethyl groups bound to the benzimidazole rings and the protons bound at the meta positions of the central pyridine ring is characteristic

(11) (a) Niori, T.; Sekine, F.; Watanabe, J.; Furukawa, T.; Takezoe, H. *J. Mater. Chem.* **1996**, *6*, 1231. (b) Niori, T.; Sekine, F.; Watanabe, J.; Furukawa, T.; Takezoe, H. *Mol. Liq. Cryst.* **1997**, *301*, 337. (c) Sekine, F.; Niori, T.; Watanabe, J.; Furukawa, T.; Chol, S. W.; Takezoe, H. *J. Mater. Chem.* **1997**, *7*, 1307.

(12) Link, D. R.; Natale, G.; Shao, R.; Maclennan, J. E.; Clark, N. A.; Körblova, E.; Walba, D. M. *Science* **1997**, *278*, 1924.

(13) (a) Heppke, G.; Moro, D. *Science* **1998**, *279*, 1872. (b) Pelzl, G.; Diele, S.; Weissflog, W. *Adv. Mater.* **1999**, *11*, 707.

(14) (a) Shen, D.; Diele, S.; Wirt, I.; Tschierske, C. *Chem. Commun.* **1998**, 2573. (b) Shen, D.; Pegenau, A.; Diele, S.; Wirth, I.; Tschierske, C. *J. Am. Chem. Soc.* **2000**, *122*, 1593.

Chart 2

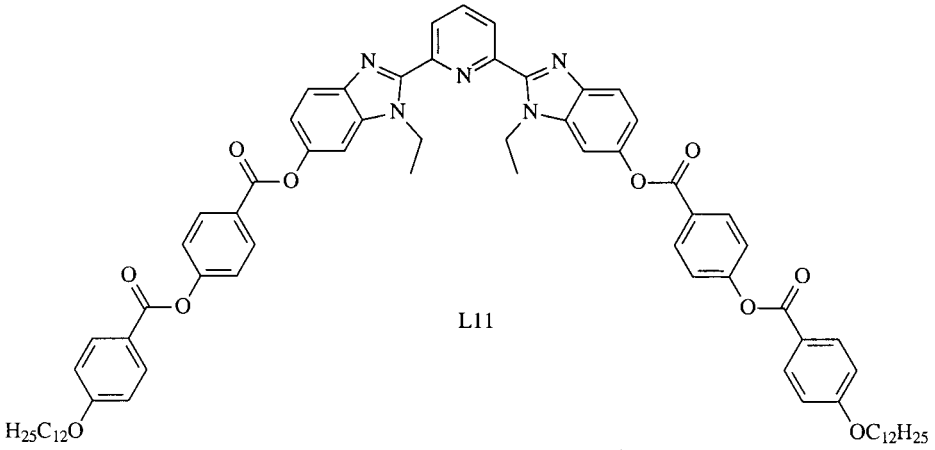

L11

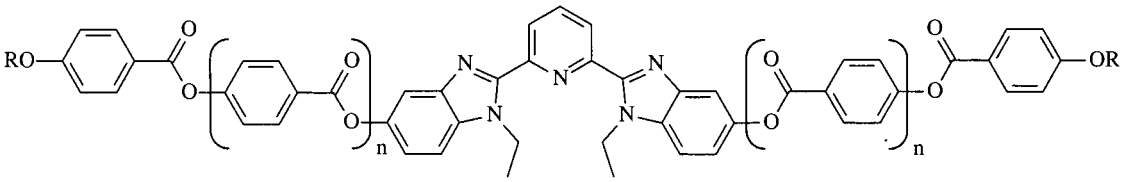

L12 : n = 1, R = $C_{12}H_{25}$
L12b : n = 1, R = C_6H_{13}
L13 : n = 2, R = $C_{12}H_{25}$

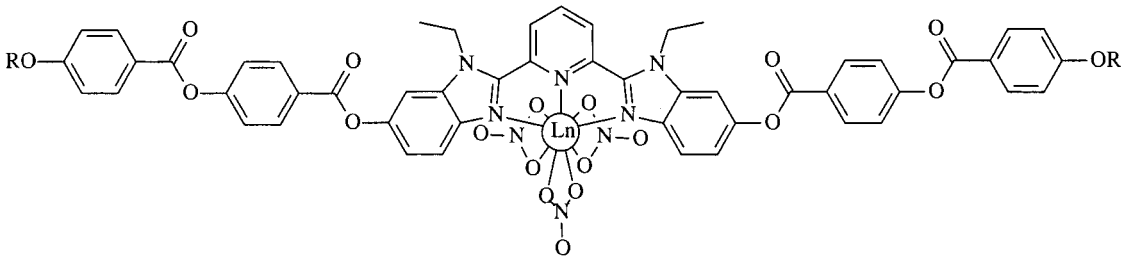

[Ln(L11)$(NO_3)_3$] (**9-13**) : R = $C_{12}H_{25}$

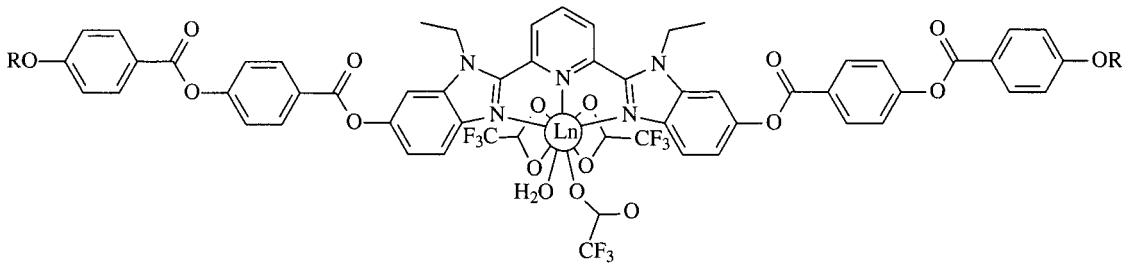

[Ln(L11)$(CF_3CO_2)_3(H_2O)$] (**14**) : R = $C_{12}H_{25}$

of the trans−trans conformation adopted by the central terdentate binding unit (i.e., the unsubstituted nitrogen atom of the benzimidazole and the nitrogen atom of the pyridine lie in a trans arrangement; Scheme 2).[8,9] We can thus propose that **L11** exhibits a V-shaped arrangement with limited axial anisometry close to that reported for **L7** and **L9**, while **L12** and **L13** display I-shaped arrangements.[8] Attempts to obtain crystals suitable for X-ray diffraction (XRD) studies failed for **L11**−**L13**, but the shorter analogue **L12b** gave appropriate single crystals.

Crystal Structures of L12b. Figure 2 shows **L12b** perpendicular to the approximate planar central terdentate core together with the atom numbering scheme. All C−C, C−N, and C−O bond distances and bond angles are standard (Table S1, Supporting Information),[16] but one terminal hexyl chain (C54−C59) is disordered and refined with two equally populated

(15) Tuffin, R. P.; Toyne, K. J.; Goodby, J. W. *J. Mater. Chem.* **1996**, *6*, 1271.
(16) Allen, F. H.; Kennard, O.; Watson, D. G.; Brammer, L.; Orpen, A. G.; Taylor, R. *J. Chem. Soc., Perkin Trans. 2* **1987**, S1.

Scheme 1[a]

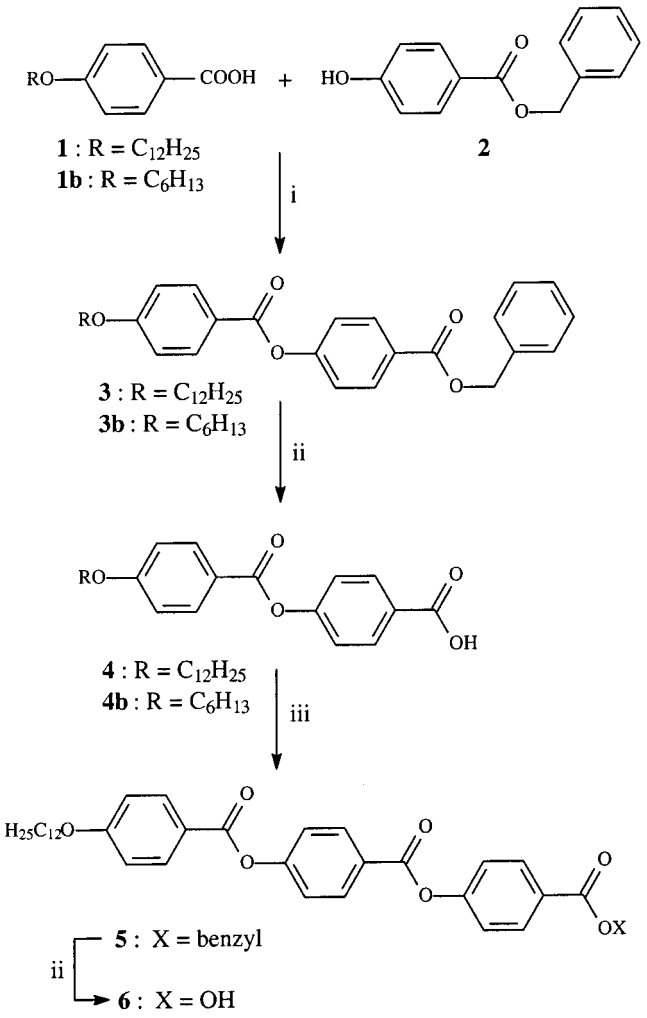

[a] Reagents: (i) DCC, DMAP, CH_2Cl_2; (ii) H_2, Pd/C, AcOEt; (iii) **2**, DCC, DMAP, CH_2Cl_2; (iv) **4**, DCC, DMAP, CH_2Cl_2; (v) **4**, **4b** (n = 1) or **6** (n = 2), DCC, DMAP, CH_2Cl_2.

Scheme 2

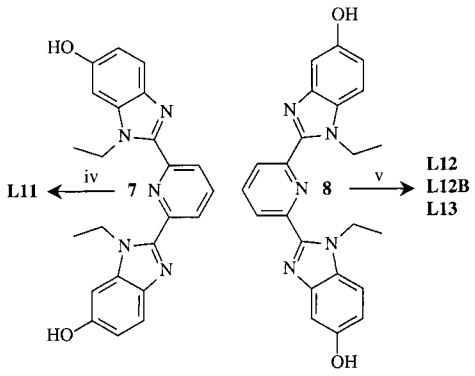

atomic sites for each carbon atom (see the Experimental Section). As previously reported for **L5** and related ligands in the solid state[8] and in agreement with solution measurements, the terdentate 2,6-bis(benzimidazol-2-yl)pyridine core adopts a trans−trans conformation associated with a minor helical twist of the three aromatic rings (interplanar pyridine−benzimidazole angles, 5.3° and 13.6°; Table S2, Supporting Information) which can be compared with 12.3° and 35.6° found for **L5**.[8] The bending of the terdentate core

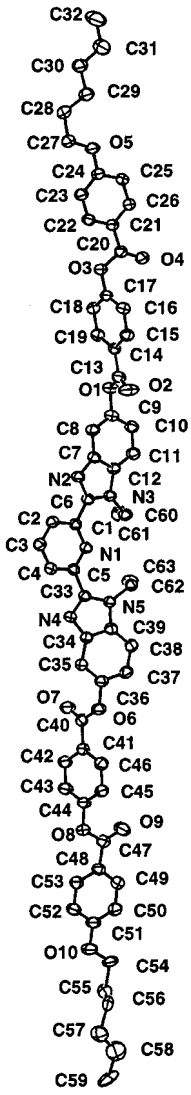

Figure 2. ORTEP[41] view of **L12b** with the atomic numbering scheme. Ellipsoids are represented at 40% probability level.

measured by the angle α(C9−N1−C36)[9] amounts to 161.4° (α = 160° for **L5**)[8] which is compatible with an almost collinear arrangement of the semirigid side arms leading to a rodlike (I-shaped) ligand. Each semirigid side arm is made up of two successive twisted phenyl rings (interplanar angles 70.9° and 78.0°) separated by a carboxylate spacer. The oxygen atom of the carbonyl group almost lies in the plane of the aromatic ring to which it is connected (deviation 0.08−0.34 Å; average 0.19 Å), and the major torsion responsible for the crossed arrangement of two successive phenyl rings results from rotation about the $C_{aromatic}$−O bonds. Related structural patterns characterize the carboxylate spacer linking the semirigid side arms to the 5 position of the benzimidazole ring of the terdentate unit (interplanar benzimidazole−phenyl angles 61.3° and 87.4°), leading to a crossed-hatched sequence of aromatic rings when moving from the benzimidazole toward the lipophilic hexyl chain (Figure 3). The length of the semirigid core between the terminal oxygen atoms (O5···O10) increases from 28.6 Å in **L5** (two phenyl rings)[8] to 41.2 Å in **L12b** (four phenyl rings; i.e., 44% of relative axial extension), while the total length of the rodlike ligand amounts to C32···C59 = 54.4 Å.

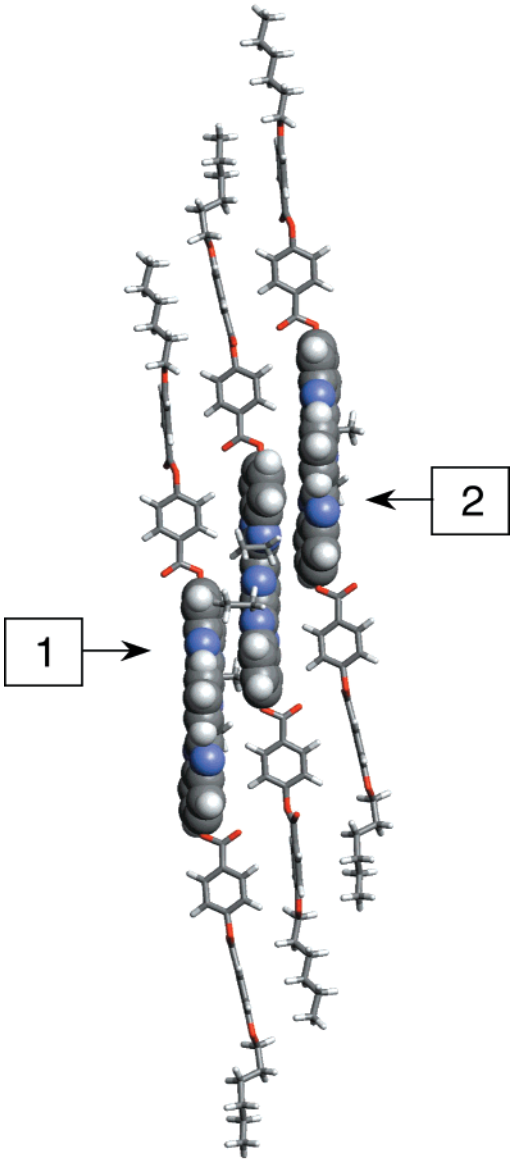

Figure 3. Perspective view of the molecular packing of **L12b** showing intermolecular stacking interactions between molecules related by inversion centers (stacking zones 1 and 2; see text).

Each approximately coplanar terdentate bis(benzimidazolyl)pyridine core is "sandwiched" between two adjacent units related to the original molecule by inversion centers, thus leading to strong head-to-tail stacking interactions between the benzimidazole rings along the [012] direction (Figure 3). The benzimidazole ring N2−N3 of **L12b** stacks [average distance 3.535(6) Å; zone 1 in Figure 3] with the related benzimidazole of the $1 - x$, $1 - y$, $1 - z$ ligand, while the benzimidazole N4−N5 interacts [average stacking distance 3.358(9) Å; zone 2 in Figure 3] with that of the $-x$, $-y$, $1 - z$ neighboring ligand. We suspect that the especially small helical twist observed for the terdentate core in **L12b** compared to that in **L5** and in related systems[8] originates from these specific intermolecular packing interactions which force a *quasi*-coplanar arrangement of the pyridine and benzimidazole rings.

Mesogenic Properties of Ligands L11−L13. The mesomorphic properties of the ligands have been investigated by a combination of differential scanning calorimetry (DSC) and polarized optical microscopy (**L11**−**L13**), together with XRD for **L11**. The rodlike ligands **L12** and **L13** display calamitic mesomorphism (Table 1) occurring at higher temperature than that previously reported for the analogue **L6** (Cr−S_C, 131 °C; S_C−S_A, 217 °C; S_A−N, 223 °C; N−I, 226 °C),[8] in line with their more elongated anisotropic structures and the associated increased intermolecular interactions. Thermogravimetric analyses indicate no significant weight loss prior to decomposition, which occurs around 320−340 °C for both ligands. The DSC traces show endotherms at 206 °C (**L12**) and 220 °C (**L13**) producing a viscous mesophase whose *schlieren* texture observed for **L13** is compatible with a smectic C mesophase as found for **L6** at lower temperature. For **L12** the birefringent texture of the mesophase cannot be reliably assigned to smectic C (Table 1). A second endotherm at 280 °C (**L12**) and >280 °C (**L13** masked by partial decomposition) leads to a nematic phase (marbled texture). Isotropization occurs around 320−340 °C, but a precise temperature is difficult to assign because of concomitant decomposition of the samples. Compared to **L6**, the main difference concerns the absence of the smectic A phase, but the highly viscous texture of the mesophase below 280 °C may hinder the observation of a S_A phase occurring in a short temperature range. For **L12b** possessing shorter hexyl chains, we observe a mesomorphism similar to that described for **L12** but within a reduced temperature range (Table 1).

The unprecedented mesogenic behavior of the V-shaped ligand **L11** is more intriguing because the

Table 1. Phase-Transition Temperatures and Enthalpy and Entropy Changes for Ligands L11−L13 and Thermal Behavior of the Complexes [Ln(L11)$(NO_3)_3$]·xH_2O (9−13) and [Ln(L11)$(CF_3CO_2)_3$·H_2O] (14)

compound	transition[a]	T/ °C	ΔH/ kJ·mol^{-1}	ΔS/ J·mol^{-1}·K^{-1}
L11	Cr−Col_R	195	28	60
	Col_R−I	203	25	52
L12	Cr^I−Cr^{II}	138	8	19
	Cr^{II}−S_x	206	33	68
	S_x−N	280	1.5	3
	N−I	322	4.5	7
L12b	Cr−S_x	187	4.7	10
	S_x−N	208	34	71
	N−I	>320[b]		
L13	Cr−S_C	220	36	73
	S_C−N	280[c]		
[La(**L11**)$(NO_3)_3$] (**9**)	Cr^I−Cr^{II}	45	10	31
	dec[d]	269		
[Eu(**L11**)$(NO_3)_3$]·$2H_2O$ (**10**)	Cr^I−Cr^{II}	56	15	45
	dec[d]	256		
[Gd(**L11**)$(NO_3)_3$]·H_2O (**11**)	Cr^I−Cr^{II}	59	15	45
	dec[d]	269		
[Tb(**L11**)$(NO_3)_3$]·$2H_2O$ (**12**)	Cr^I−Cr^{II}	48	12	37
	dec[d]	262		
[Lu(**L11**)$(NO_3)_3$]·H_2O (**13**)	dec[d]	258		
[Lu(**L11**)$(CF_3CO_{12})_3$·H_2O] (**14**)	Cr^I−Cr^{II}	69	90	260
	Cr^{II}−I	221	67	135

[a] Cr = crystal, S_C = smectic C phase, S_x = undetermined smectic phase, N = nematic phase, Col_R = rectangular columnar phase, and I = isotropic fluid. Temperatures are given as the onset of the peak observed during heating processes (Seiko DSC 220C differential scanning calorimeter, 5 °C·min^{-1}, under N_2). The liquid crystalline phases were identified from their optical textures: S_C = broken focal-conic fan and *Schlieren* textures; N = *Schlieren* and marbled textures. [b] Isotropization masked by decomposition (see text). [c] Decomposition concomitant with the formation of the nematic phase (see text). [d] Decomposition.

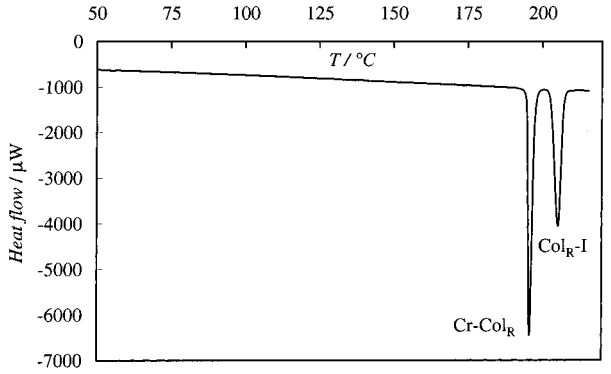

Figure 4. DSC trace of **L11** (second heating, 5 °C·min^{-1} under N_2).

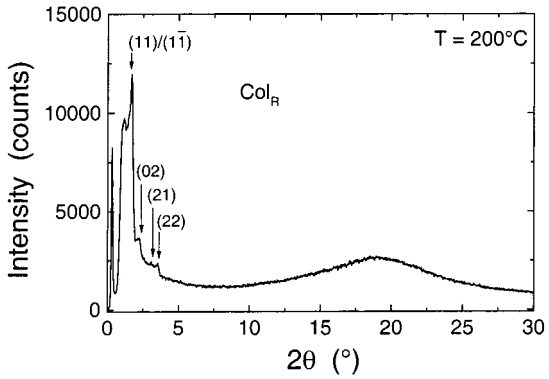

Figure 5. Scattering diagram of a nonoriented sample of **L11** in the Col$_R$ phase (200 °C).

Table 2. Observed and Calculated Scattering Vectors for L11 in the Col$_R$ Mesophase at 200 °C (Space Group *P*2*mg*, a = 59.8 Å, b = 74.5 Å, γ = 90°, s = 4455 Å^2)

θ_{obs}	d_{obs}	intensity	hk	θ_{calc}	d_{calc}
0.94	46.6	vs	11/1$\bar{1}$	0.95	46.6
1.19	37.2	s	02	1.19	37.2
1.61	27.5	vw	21	1.59	27.7
1.86	23.7	vw	22	1.89	23.3
9.6	4.6	w	diffuse	9.64	4.6

lighter analogue **L7** displays no mesomorphism and melts to the isotropic liquid at 154 °C.[9] The DSC trace of **L11** displays two successive endotherms with comparable enthalpies at 195 and 203 °C (heating mode; Figure 4) and 203 and 183 °C (cooling mode). The mesophase can be detected by the formation of crumpled fans together with an intercalar fine mosaic texture (Figure S3, Supporting Information). XRD scattering diagrams collected in the 200−188 °C range confirm the formation of an organized mesophase (Figure 5 and Table 2). A wide-angle diffuse scattering centered at ca. 4.6 Å, characteristic of the aliphatic chains in their molten state and corresponding to a short-range order of the molecules, is observed together with a series of sharp, nonequidistant Bragg reflections in the small-angle region (Figure 5). These reflections can be indexed with the Miller index pairs hk = (11)/(1$\bar{1}$), (20), (21), and (22) and correspond to a two-dimensional rectangular lattice characteristic of a rectangular columnar mesophase Col$_R$. Because the (21) reflection, although weak, is observed, there are no reflection conditions on the hk Miller indices (Table 2).

The a parameter (59.8 Å) of the rectangular cell is in good agreement with the length of the molecule (L = 61.7 Å) estimated for a central bent angle of 120° (Figure 6a: the total length of the rigid core (41.2 Å) is taken from the crystal structure of **L12b** and the length of the extended *all-trans*-dodecyl chain (≈15 Å) from the crystal structure of **L5**).[8] A ribbon of parallel and aligned bent-core molecules is likely for this columnar mesophase where a is the thickness of the ribbon and b = 74.5 Å is the periodicity in the perpendicular direction. These ribbons arrange in a two-dimensional lattice close to that proposed by Diele and collaborators for related compounds **L8**−**L10** in their Col$_R$ mesophase (Figure 6b).[14] The molecular volume of **L11** can be calculated according to $V_m = (M_w \times 10^{24})/dN_A$ = 2025 Å^3 (M_w is the molecular weight of **L11** (1217 g/mol), d is the density of the mesophase estimated to 1.0 g/cm^3 for a purely organic molecule (d = 1.294 g/cm^3 for the more compact ligand **L12b** and 1.19 g/cm^3 for **L5** in the crystalline phase at 200 K),[8] and N_A is Avogadro's number), and it can be compared to the volume of the unit cell $V_{cell} = abh$ = 20 500 Å^3, where h is the periodicity along the columnar axis corresponding to the average intermolecular distance between the molecules (h = 4.6 Å). We deduce that the average number of molecules per unit cell is $N_{cell} = V_{cell}/V_m = 10$. To escape macroscopic polar order, clusters of $N_{cell}/2 = 5$ molecules of neighboring ribbons adopt an antiparallel arrangement (Figure 6b).[14] The *P*2*mg* (No. 7) plane group is fully compatible with this antiferroelectric motif, with each cluster being located on a mirror plane (special position 2c) that does not provide extra conditions for the reflection in agreement with the observation of the (21) reflection in the XRD profile. Because half of the rigid core (20.6 Å) in **L11** is longer than one extended dodecyloxy chain (15 Å), we expect significant overlap between the terminal aromatic rings of antiparallel

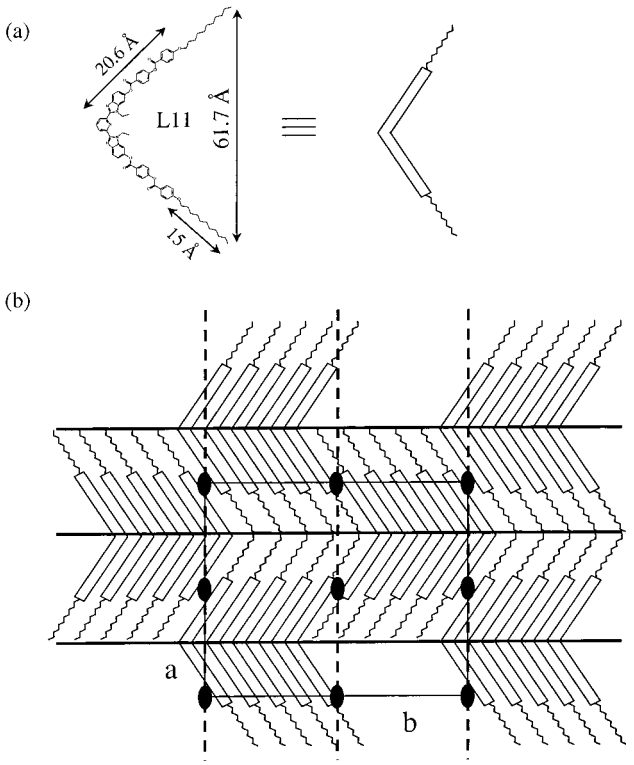

Figure 6. (a) Estimated molecular anisometry of the bent ligand **L11**. (b) Structure model of the Col$_R$ phase with representations of the unit cell and associated symmetry elements (space group *p*2*mg*).

Table 3. Ligand-Centered Absorption and Emission Properties of Ligands L11−L13 and Compound 4 [10^{-5} M in CH_3CN/CH_2Cl_2 (7:3)] at 298 K

compound	$\pi \rightarrow \pi^*$ absorption/cm^{-1}	$^1\pi\pi^*$ emission/cm^{-1}	λ_{exc}/nm
L11	37 450 (73 500)[a]	22 730	321
	31 150 (39 700)		
L12	37 300 (94 400)	23 700	325
	30 770 (42 800)		
	25 700 (9430 sh)		
L13	36 200 (113 000)	23 580	334
	30 770 (39 600)		
	26 110 (11 000 sh)		
4	37 880 (26 850)	*b*	
	36 630 (23 800 sh)		

[a] Energies are given for the maximum of the band envelope in cm^{-1}, and the molar absorption coefficient (ϵ) is given in parentheses in $M^{-1}\cdot cm^{-1}$; sh = shoulder. [b] Too weak to be measured.

molecules at the ribbon interface which are thought to stabilize the Col_R phase (Figure 6b).[13,14]

Photophysical Properties of Ligands L11−L13. The introduction of sequences of phenyl rings separated by carboxylate spacers not only provides new intermolecular interactions stabilizing specific arrangements of the molecules in the solid state and in the mesophases but also affects the photophysical properties of the resulting ligands, a crucial point if these receptors have to be used as UV-light harvesters in luminescent lanthanide-containing materials. Previous detailed photophysical investigations of **L4**, **L5**, and **L7** combined with semiempirical ZINDO calculations[17] applied on PM3-optimized[18] gas-phase geometries have established that (i) the ligands **L4**, **L5**, and **L7** adopt trans−trans conformations of the bis(benzimidazolyl)pyridine units associated with absorption and emission spectra dominated by $\pi \rightarrow \pi^*$ transitions (15 000−40 000 cm^{-1}) centered on the terdentate bent core and (ii) the connection of π-donor atoms to the 5 (**L5**) or 6 (**L7**) position of the benzimidazole ring raises the HOMO (and SHOMO) without significantly perturbing LUMO (and SLUMO), thus producing a red shift of the $\pi \rightarrow \pi^*$ transitions in the order **L4** < **L7** < **L5**.[8,9] Except for a better resolution in solution, the absorption spectra of **L11**−**L13** are similar in solution (Table 3) and in the solid state (Table 4), pointing to trans−trans conformations of the terdentate binding units in both states. **L11**−**L13** exhibit broad and intense absorption bands which can be separated into two categories: one envelope at low energy centered around 30 800 cm^{-1} (with a low-energy shoulder for **L12** and **L13** around 26 000 cm^{-1}) as similarly observed for **L4** (31 050 cm^{-1})[8] and **L6** (30 770 cm^{-1})[8] and a second envelope at higher energy which has no counterpart in **L4**−**L7** (Figure 7 and Tables 3 and 4).

The C_2-constrained gas-phase geometries of the rigid cores of **L11** and **L12** (the dodecyl chains are replaced by methyl termini in order to limit excessive computing)[9] optimized with the semiempirical AM1 method[19] also predict trans−trans arrangements of the terdentate binding units which result from (i) the minimization of steric constraints between the ethyl substituents borne by the benzimidazole rings, (ii) the repulsion between the dipolar moments of the nitrogen lone pairs,[20] and (iii) the maximization of π overlap.[6] The predicted interplanar pyridine−benzimidazole angles (44.1° for **L11** and 42.3° for **L12**) are larger than those found in the solid state, thus highlighting the effect of intermolecular packing forces in the crystal structure of **L12b** (Figure 3). This remark also holds for the crosshatched arrangements of the successive phenyl rings of the side arms (interplanar angles 61.3−87.4° in the crystal structure of **L12b**) which are only qualitatively reproduced by the modeling in the gas phase (benzimidazole−phenyl, 54.4−55.6°; phenyl−phenyl, 45.2−45.3°). ZINDO calculations[17] performed on these optimized geometries predict several close and intense $\pi \rightarrow \pi^*$ transitions at low energies (29 310−34 800 cm^{-1} for **L11** and 29 140−33 370 cm^{-1} for **L12**) involving frontier orbitals exclusively centered on the terdentate binding units (Tables S3−S6, Supporting Information) as previously reported for **L4**, **L5**, and **L7**.[9] The low-energy envelope observed in the absorption spectra of **L11**−**L13** can thus be assigned to these $\pi \rightarrow \pi^*$ transitions. The connection of the poor electroattracting carboxylate spacer at the 6 (**L11**) or 5 position (**L12**) produces comparable HOMO−LUMO (and SHOMO−SLUMO) gaps, leading to $\pi \rightarrow \pi^*$ transitions at similar energies for both ligands (Figure S1, Supporting Information), in good agreement with experimental data (Figure 7a). The intense envelope at higher energy can be ascribed to $\pi \rightarrow \pi^*$ transitions centered on the aromatic phenyl groups connected by carboxylate spacers in the side arms according to ZINDO calculations [maximum of the band envelopes expected at 41 700 cm^{-1} (**L11**) and 40 080 cm^{-1} (**L12**)]. This tentative assignment is strongly supported by (i) the experimental absorption spectra of **L6**, which only matches the low-energy part of the spectra observed for **L12**, and (ii) the single maximum observed at 37 880 cm^{-1} for the precursor of the side chain **4** (Figure 7a). We thus conclude that the almost perpendicular arrangement of the phenyl rings connected to the benzimidazole prevents efficient electronic communication between side arms and the central core despite the replacement of ether spacers of **L4**, **L5**, and **L7** by carboxylate spacers in **L11** and **L12**.

The emission spectra of **L11**−**L13** (10^{-5} M in CH_3CN/CH_2Cl_2, 7:3) display weak Stokes-shifted and poorly structured bands arising from $^1\pi\pi^*$ excited states at 22 730 cm^{-1} (**L11**) and 23 700 cm^{-1} (**L12** and **L13**), which can be compared to 23 640 cm^{-1} for **L6** under the same conditions (Figure 7b),[8] but emission from the triplet states escapes detection in solution. The emission spectra of **L12** and **L13** in the solid state (77 K) qualitatively match those found in solution (0−0 phonon transitions given in Table 4), but the main component of the $^1\pi\pi^*$ emission of **L11** in the solid state appears as a poorly structured band red-shifted by 5115 cm^{-1} compared to **L12** and assigned to excimer emission arising from close intermolecular packing interactions between aromatic rings according to the theory of Stevens and Ban.[21] Closely related effects have been recently reported by Kitzerow and co-workers for closely

(17) Zerner, M. C. *ZINDO Manual*; QTP, University of Florida: Gainesville, FL, 1990. Broo, A.; Pearl, G. M.; Zerner, M. C. *J. Phys. Chem.* **1997**, *101*, 2478. Siegbahn, P. E.; Heidberg, A.; Roos, B. O.; Levy, B. *Phys. Ser.* **1980**, *21*, 323.
(18) Stewart, J. J. P. *J. Comput. Chem.* **1989**, *10*, 209, 221.
(19) Dewar, M. J. S.; Zoebisch, E. G.; Healy, E. F. *J. Am. Chem. Soc.* **1985**, *107*, 3902.
(20) Case, F. H.; Kasper, T. J. *J. Am. Chem. Soc.* **1956**, *78*, 5842.
(21) Stevens, B.; Ban, M. I. *Trans. Faraday Soc.* **1964**, *60*, 1515.

Table 4. Ligand-Centered Absorption and Emission Properties of Compound 4, Ligands L11−L13 and Complexes [Ln(L11)(NO$_3$)$_3$] (9−13) in the Solid State[a]

compound	$\pi \rightarrow \pi^*$ absorption/cm^{-1}	$^1\pi\pi^*$ emission/cm^{-1}	$^3\pi\pi^*$ emission/cm^{-1}	τ ($^3\pi\pi^*$) lifetime/ms
4	37 040	32 470	24 510	*b*
		28 410	23 200	
L11	37 735	21 410	22 675	247(18)
	30 770	20 325	20 620	5.3(8)
			19 340	
			17 950	
L12	37 735	26 525 sh	25 000	606(3)
	30 770	25 190	24 090	26.3(7)
	25 840 sh	24 210	20 370	
			19 960	
			19 380	
			17 920	
L13	37 740	26 525	25 000	575(20)
	30 770	25 840	23 530	14(7)
	25 840 sh	24 570 sh	19 920	
			18 870	
			17 740	
[La(**L11**)(NO$_3$)$_3$] (**9**)	37 735	25 000	23 520	148(2)
	27 030	23 870	21 050	20.6(3)
	23 530 sh		19 050	
			18 020	
[Gd(**L11**)(NO$_3$)$_3$] (**11**)	37 735	25 250	20 325	2.8(1)
	27 030		18 250	0.75(7)
			16 860	
			16 100	
[Lu(**L11**)(NO$_3$)$_3$] (**13**)	37 735	25 250	23 810	61(5)
	27 030		22 220	5.5(3)
	23 530 sh		19 610	
			18 180	
			16 670	
[Eu(**L11**)(NO$_3$)$_3$] (**10**)	37 735	*b*	*c*	*c*
	27 030			
[Tb(**L11**)(NO$_3$)$_3$] (**12**)	37 735	*b*	*c*	*c*
	27 030			

[a] Reflectance spectra recorded at 295 K, luminescence data at 77 K, and lifetime measurements at 20 K (λ_{exc} = 308 nm); sh = shoulder. [b] Too weak to be measured. [c] $^3\pi\pi^*$ luminescence quenched by transfer to the Ln ion.

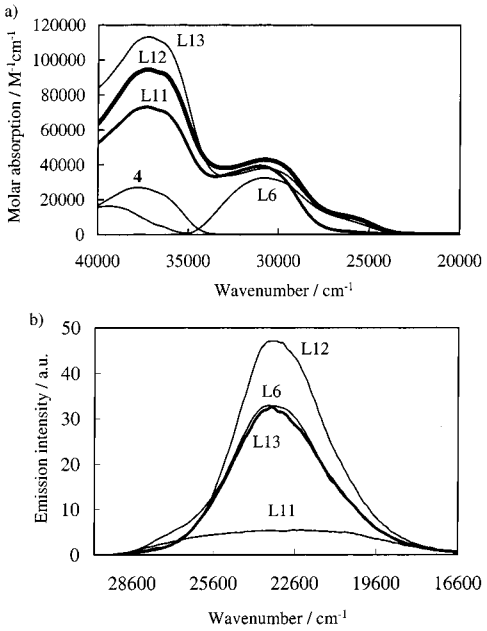

Figure 7. (a) Absorption and (b) emission spectra of **L6**, **L11**, **L12**, **L13**, and **4** (10^{-5} M) in CH_3CN/CH_2Cl_2 (7:3) at 298 K (λ_{exc} are given in Table 3).

packed fluorescent columnar liquid crystals possessing substituted perylene units.[22] The excitation spectra of **L11**−**L13** obtained by monitoring the $^1\pi\pi^*$ emission match the low-energy part of the absorption spectra assigned to excited states centered on the terdentate binding unit, which implies a very limited funneling of the energy collected by the side arms toward the central terdentate core. Time-resolved emission spectra (delay time 0.1−0.8 ms) reveal complicated and faint, but structured, emission originating from the $^3\pi\pi^*$ states. Compared to related emission in **L6** (0−0 phonon, 19 380 cm^{-1}; monoexponential decay τ = 614 ms at 10 K),[8] the phosphorescence spectra of **L11**−**L13** at 20 K cover a significantly broader domain (25 000−15 400 cm^{-1}) with 0−0 phonon transitions at significantly higher energies (Table 4). Biexponential decay is systematically observed, with a long-lived component (250−600 ms at 20 K; Table 4) comparable to that observed for **L6** and a short component (5−26 ms) that has no counterpart in **L6**. Interestingly, the high-energy 0−0 phonon transitions of **L11**−**L13** match that observed for the extremely faint $^3\pi\pi^*$ emission from the side arm **4** (24 510 cm^{-1}). These results suggest that the delayed emission spectra of **L11**−**L13** originate from two different triplet states, one associated with the terdentate binding unit, centered around 20 000 cm^{-1}, with a long lifetime and the second one associated with the appended polyaromatic side arms occurring at higher energy and with a shorter lifetime. Because of the extremely weak intensity of the time-resolved spectra, the associated excitation spectra were not accessible with our experimental setup. We conclude that the photophysical properties of the side arms parallel those

(22) Benning, S.; Kitzerow, H.-S.; Bock, H.; Achard, M.-F. *Liq. Cryst.* **2000**, *27*, 901.

of the terdentate binding units in **L11**−**L13** because of the significant extension of the aromatic side arms, which contrasts with **L4**−**L7,** for which only excited states centered on the terdentate binding units are accessible for energies below 40 000 cm^{-1}.

Synthesis, Characterization, and Thermal Behavior of the Complexes [Ln(L11)$(NO_3)_3$]·xH_2O (Ln = La, x = 0, 9; Ln = Eu, x = 2, 10; Ln = Gd, x = 1, 11; Ln = Tb, x = 2, 12; Ln = Lu, x = 1, 13) and [Lu(L11)$(CF_3CO_2)_3$·H_2O] (14). The bent-core mesomorphic ligand **L11** has been selected for the investigation of extended rodlike 1:1 lanthanide complexes because the meridional coordination of the terdentate binding unit and the associated trans−trans → cis−cis conformational change transform the V-shaped ligand into an I-shaped receptor, as was previously demonstrated in the crystal structures of [Lu(**L7**)$(NO_3)_3$] and [Lu(**L7**)-$(CF_3CO_2)_3]_2$ (Figure 1 and Chart 2).[9] The mixing of stoichiometric quantities of **L11** and Ln$(NO_3)_3$·xH_2O (x = 2−6) or Lu$(CF_3CO_2)_3$·H_2O in acetonitrile/dichloromethane followed by crystallization in hot propionitrile or butyronitrile gives the complexes [Ln(**L11**)-$(NO_3)_3]$·xH_2O (Ln = La, x = 0, **9**; Ln = Eu, x = 2, **10**; Ln = Gd, x = 1, **11**; Ln = Tb, x = 2, **12**; Ln = Lu, x = 1, **13**) and [Lu(**L11**)$(CF_3CO_2)_3$·H_2O] (**14**) in good yields (74−85%). The IR spectra of complexes **9**−**13** are dominated by the vibrations of the ligand backbone, together with bands characteristic of coordinated bidentate nitrates, as was previously discussed for [Ln(**L7**)$(NO_3)_3$].[9] The stretching vibrations of the carbonyl groups in **9**−**13** display two bands at 1730 and 1685 cm^{-1}, which have no counterpart in [Ln(**L7**)$(NO_3)_3$] possessing ether spacers. A related IR spectrum is observed for **14**, but the nitrates and their typical vibrations are replaced by vibrations associated with the trifluoroacetates.[9] The asymmetric stretching vibrations of $CF_3CO_2^-$ (1740−1620 cm^{-1}) overlap with the ν(C═O) vibrations of the carboxylate spacers except for an extra band at 1635 cm^{-1} assigned to one component of $\nu_{as}(CO_2^-)$ typical of bound trifluoroacetate anions in [Lu(**L11**)$(CF_3CO_2)_3$·H_2O] (**14**).[23] The thermal behavior of the nitrato complexes **9**−**12** shows a reversible transition at low temperature (45−59 °C; Table 1) assigned to a crystal−crystal phase transition (polarizing microscopy). Further heating leads to isotropization in the range 256−258 °C, closely followed by the exothermic decomposition of the melted oxidizing nitrate salts, as was similarly observed for [Ln(**L7**)$(NO_3)_3$] in the range 184−198 °C.[9] We thus obtain a similar thermal behavior for lanthanide nitrato complexes with **L7** and **L11**, except for a shift of ca. 60 °C of the isotropization process toward higher temperatures for the heavier complexes **9**−**12**. The Lu complex **13** displays a similar behavior (isotropization followed by decomposition at 258 °C), but no Cr^{I}−Cr^{II} phase transition is observed at lower temperature. Finally the replacement of NO_3^- by $CF_3CO_2^-$ in [Lu(**L11**)$(CF_3CO_2)_3$·H_2O] (**14**) prevents decomposition in the liquid (221 °C), but no mesogenic behavior can be detected by polarizing microscopy.

Crystal Structure of [Lu(L11)$(CF_3CO_2)_3$·H_2O] (14). The crystal structure of **14** shows it to be composed of centrosymmetric dimers in which two [Lu(**L11**)$(CF_3CO_2)_3$·H_2O] complexes are connected by four hydrogen bonds involving the coordinate water molecule and the monodentate trifluoroacetate anions. Figure 8 shows the monometallic unit [Lu(**L11**)$(CF_3CO_2)_3$·H_2O], Figure 9 shows a stereoscopic view of the H-shaped hydrogen-bonded dimer, and Figure 10 focuses on the hydrogen-bonding network. Selected bond distances and bond lengths are collected in Table 5.

The terdentate core in [Lu(**L11**)$(CF_3CO_2)_3$·H_2O] adopts the expected quasi-planar cis−cis conformation (interplanar pyridine−benzimidazole angles 11.6° and 28.9°; Table S7, Supporting Information) resulting from its meridional tricoordination to Lu(III).[8,9] The associated interconversion of the 5 and 6 positions of the benzimidazole rings occurring upon complexation[9] thus transforms the V-shaped ligand **L11** into an I-shaped extended receptor in **14** with a geometrical anisometry comparable to that found in **L12b** except for a minor scissoring effect which reduces the angle α(C10−N1−C45) from 161.4° in **L12b** to 137.5° in [Lu(**L11**)$(CF_3CO_2)_3$·H_2O], as was similarly described for [Lu(**L7**)-$(NO_3)_3]$ (α = 134.4°) and [Lu(**L7**)$(CF_3CO_2)_3]_2$ (α = 138.4°).[9] The almost parallel arrangement of the *all-trans*-alkyl chains in **14** (deviation 4.5°) running in opposite directions demonstrates that the decrease of ca. 25° in the bending angle α when going from the free ligand **L12b** to the complexed receptor **L11** in **14** can be compensated for by the flexibility of the semirigid side arms. Rotations about the $C_{aromatic}$−O bonds of the carboxylate spacers produce a crosshatched arrangement of the successive benzimidazole and phenyl rings with interplanar angles (41.8−64.4°; Table S7, Supporting Information) comparable to those found for **L12b** (61.3−87.4°), eventually providing similar I-shaped conformation and axial anisometry of the semirigid aromatic cores in **L12b** and [Lu(**L11**)$(CF_3CO_2)_3$·H_2O] (Figure 9): (i) length of the semirigid core O5···O10 = 40.2 Å in **14** (41.2 Å for **L12b**), (ii) total length of the extended dodecyl receptor C38···C73 = 70.3 Å in **14** (71.2 Å for **L12**), and (iii) approximate thickness of the ligand backbone C9···C40 = 5.7 Å in **14** (5.8 Å for **L12b**). The lutetium ion is eight-coordinated in a low-symmetry coordination environment defined by three nitrogen atoms of the terdentate binding units (Lu−N = 2.428−2.507 Å; average 2.47 Å), one bound bidentate trifluoroacetate [Lu−O = 2.394(5) and 2.437(4) Å], two monodentate trifluoroacetates [Lu−O = 2.192(6) and 2.194(4) Å], and one water molecule [Lu−O1 = 2.281(5) Å]. All bond distances are standard and closely match those found for [Lu(**L7**)$(CF_3CO_2)_3]_2$.[9] As previously noticed, monodentate and bridging $CF_3CO_2^-$ anions provide Lu−O bond distances shorter than those observed for bidentate $CF_3CO_2^-$ and the Lu−O(water) bond fits those reported for $[Lu(CF_3CO_2)_3(OH_2)_3]_2$.[25] Lu(III) lies slightly out of a basal plane defined by the coordinated nitrogen atoms (deviation 0.166 Å toward the bidentate trifluoroacetate). The bidentate and one monodentate trifluoroacetate (c) are located on opposite sides of this plane, and the remaining monodentate anion (trifluoroacetate b) and the water molecule occupy roughly equatorial

(23) Giorgetti, A.; Bünzli, J.-C. G. *Inorg. Chim. Acta* **1985**, *110*, 225 and references therein.

(24) Piguet, C.; Williams, A. F.; Bernardinelli, G.; Moret, E.; Bünzli, J.-C. G. *Helv. Chim. Acta* **1992**, *75*, 1697. Guerriero, P.; Vigato, P. A.; Bünzli, J.-C. G.; Moret, E. *J. Chem. Soc., Dalton Trans.* **1990**, 647.

(25) Junk, P. C.; Kepert, C. J.; Wei-Min, L.; Skelton, B. W.; White, A. H. *Aust. J. Chem.* **1999**, *52*, 459.

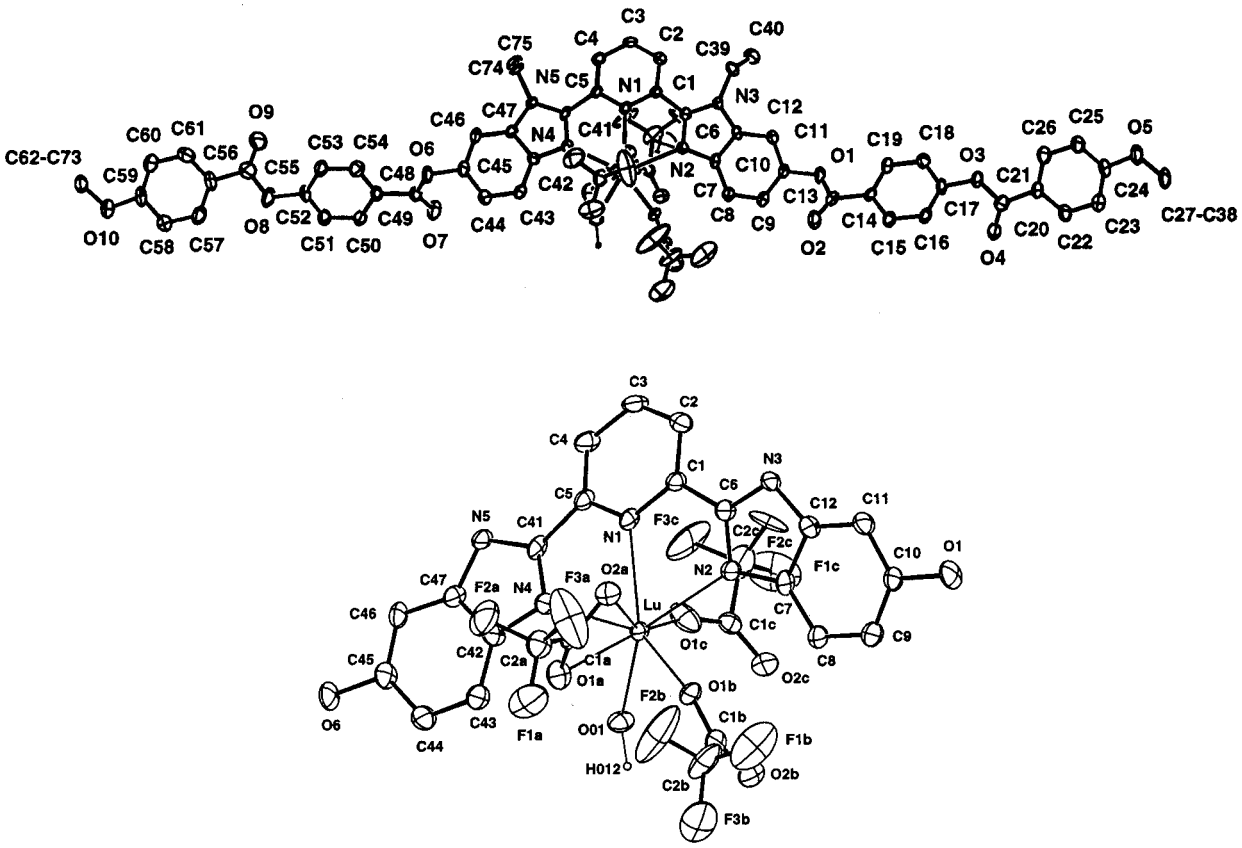

Figure 8. ORTEP[41] view of [Lu(**L11**)$(CF_3CO_2)_3(H_2O)$] (**14**) with an atomic numbering scheme. Ellipsoids are represented at 40% probability level.

positions (0.80 and −0.75 Å out of the basal plane). This geometry strongly contrasts with the nine-coordinated Lu(III) found in [Lu(**L7**)$(CF_3CO_2)_3]_2$, in which two bidentate $CF_3CO_2^-$ occupy axial positions while two bridging trifluoroacetate lie in the equatorial plane, leading to a centrosymmetrical dimer with a short Lu⋯Lu distance [5.067(1) Å].[9] In **14**, a related loosely bound centrosymmetrical H-shaped dimer [Lu(**L11**)$(CF_3CO_2)_3\cdot H_2O]_2$ [Lu⋯Lu = 6.2859(5) Å] results from a network of four hydrogen bonds involving each coordinated water molecule acting as a donor of two separated hydrogen bonds toward the accepting free oxygen atoms of the monodentate trifluoroacetates of the neighboring molecule (Figure 10). The $O_{donor}\cdots O_{acceptor}$ distances [O1⋯O2b′ = 2.706(8) Å and O1⋯O2c′ = 2.714(7) Å] together with $O_{donor}-H\cdots O_{acceptor}$ angles [168(7)° and 167(6)°, respectively] and $O_{donor}-H$ bond distances [O1−H11 = 0.88(9) Å and O1−H12 = 1.07(7) Å] are in line with standard values for O−H⋯O bonds[26] exhibiting minor proton transfer.[27]

The thickness of the ellipsoidal core produced by the coordination spheres of the metals in the H-shaped dimer [Lu(**L11**)$(CF_3CO_2)_3\cdot H_2O]_2$ along the two directions perpendicular to the long molecular axis of the receptors amounts to 12.90 Å (C2a⋯C2a′) and 15.35 Å (C3⋯C3′), leading to length-to-width ratios of 5.5 and 4.6, somewhat larger than the value 3.9 found for [Lu(**L7**)$(CF_3CO_2)_3]_2$.[9] Finally, the H-shaped dimers of **14** adopt a parallel arrangement in the crystal, with their long molecular axis running along the [11$\bar{3}$] direction and forming layers approximately perpendicular to the *c* direction. Within a layer, two neighboring dimers are systematically offset by ca. 8 Å, and packing of these layers provides closest interdimer Lu⋯Lu distances of 10.498 Å, but we do not detect significant π-stacking interactions in the unit cell (Figure S2, Supporting Information).

Photophysical Properties of Complexes [Ln(L11)$(NO_3)_3]\cdot xH_2O$ (Ln = La, *x* = 0, 9; Ln = Eu, *x* = 2, 10; Ln = Gd, *x* = 1, 11; Ln = Tb, *x* = 2, 12; Ln = Lu, *x* = 1, 13). The poor solubility of complexes **9**−**13** in organic solvents limits the photophysical study to microcrystalline samples in the solid state. Upon complexation of **L11** to Ln(III) in **9**−**13**, the low-energy $\pi \rightarrow \pi^*$ transitions centered on the terdentate core are split and red-shifted by 3740 cm^{-1} (Table 4), as was previously reported for [Ln(**L7**)$(NO_3)_3]$ (2500 cm^{-1})[9] and assigned by EHMO calculations to the trans−trans → cis−cis conformational change associated with meridional coordination of the ligand.[28] The high-energy $\pi \rightarrow \pi^*$ transitions centered on the semirigid aromatic side arms (37 735 cm^{-1}) are not affected by complexation because the carboxylate spacers do not interact with the metal, as was demonstrated in the crystal structure of **14**. The $^1\pi\pi^*$ emission of the coordinated ligand in the La, Gd, and Lu complexes appears as weak, broad, and poorly structured bands in the spectra at 77 K, with 0−0 phonon transitions around 25 000 cm^{-1} (Table 4), at significantly higher energy than those found for the

(26) Ceccarelli, C.; Jeffrey, G. A.; Taylor, R. *J. Mol. Struct.* **1981**, *70*, 255.
(27) Joesten, M. D. *J. Chem. Educ.* **1982**, *59*, 362.
(28) Piguet, C.; Bünzli, J.-C. G.; Bernardinelli, G.; Bochet, C. G.; Froidevaux, P. *J. Chem. Soc., Dalton Trans.* **1995**, 83−97.

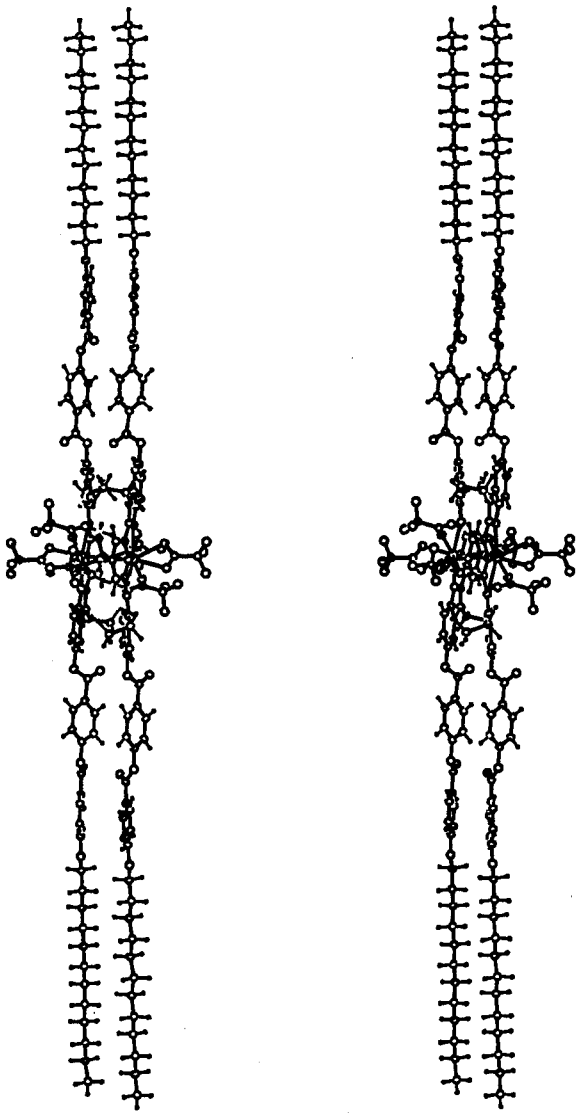

Figure 9. Perspective stereoview of complex **14** showing the centrosymmetrical H-shaped dimer.

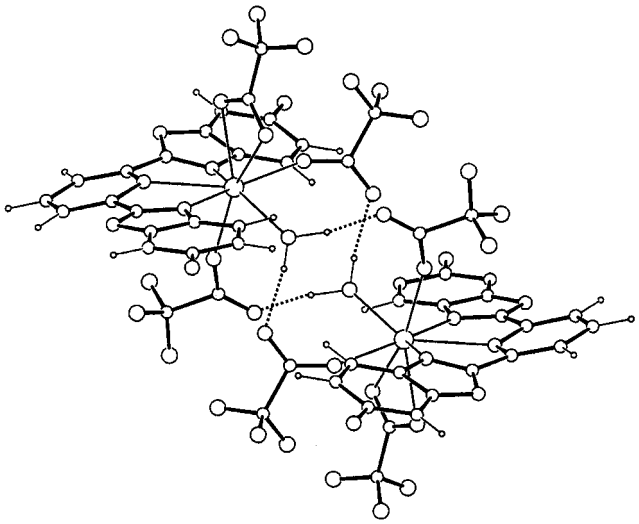

Figure 10. Perspective view of the coordination sphere of **14** showing the network of hydrogen bonds in the H-shaped dimer.

analogous complexes with **L7** (21 230−22 400 cm^{-1}).[9] The ligand-centered $^3\pi\pi^*$ emission (delay time 0.1−1 ms) is faint for the three complexes **9**, **11**, and **13**, and it also displays broad and poorly structured bands in the range 16 000−25 000 cm^{-1} (Table 4). The emission decay at 20 K is biexponential (ν_{an} = 19 230 cm^{-1}), exhibiting long and short components (Table 4), a behavior closely related to that of the $^3\pi\pi^*$ emission of the free ligand under the same conditions and assigned to different triplet excited states centered on the terdentate core and on the appended aromatic side arms, respectively. The observation of monoexponential decays for $^3\pi\pi^*$ emissions in [Ln(**L7**)$(NO_3)_3$] (τ = 111 (La), 1.33 (Gd), and 57.1 (Lu) ms)[9] strongly supports this interpretation. The reduced lifetimes associated with paramagnetic Gd(III) have been previously documented.[29] In [Eu(**L11**)$(NO_3)_3]\cdot 2H_2O$ (**10**), efficient **L11** → Eu(III) energy-transfer processes quench the ligand-centered emission and produce a bright red luminescence (20−295 K) originating from Eu-centered $^5D_0 \rightarrow {}^7F_j$ (j = 1−4) transitions (Figure S4, Supporting Information). The high-resolution $^5D_0 \leftarrow {}^7F_0$ excitation profile at 20 K displays a major sharp component at 17 227 cm^{-1} (full width at half-height fwhh = 2.1 cm^{-1}) together with two shoulders at higher (17 230 cm^{-1}) and lower energy (17 224 cm^{-1}), respectively, suggesting the existence of three slightly different crystalline sites (Figure S5, Supporting Information). However, the emission spectra obtained under selective excitation are very similar, pointing to only minor differences between the metallic environments in agreement with polydispersion within a microcrystalline sample.[24,29] The $^5D_0 \leftarrow {}^7F_0$ excitation profile is broader at 295 K (fwhh = 7 cm^{-1}), leading to a single transition at 17 239 cm^{-1}, the energy of which somewhat deviates from the one predicted by the empirical equation proposed by Frey and Horrocks[30] for Eu(III) nine-coordinated by three heterocyclic nitrogen atoms (17 248 cm^{-1} at 295 K).[9] The nephelauxetic effect is, however, very sensitive to bond lengths, and the observed deviation may arise from this factor. Excitation spectra in the UV domain obtained upon monitoring $^5D_0 \rightarrow {}^7F_2$ show a maximum around 26 300 cm^{-1}, which matches the low-energy envelope of the absorption spectrum corresponding to excited states centered on the terdentate unit. Excitation to higher energy states centered on the semirigid side arms resulted in no detectable Eu-centered emission consistent with the conclusion that the coordinated terdentate binding units are the major antennae for sensitizing the luminescence of Eu(III) in **10**. The Eu($^5D_0$) lifetime amounts to ca. 1.1 ms and is temperature independent in the range 20−295 K (Table S8, Supporting Information), which indicates that the $^3\pi\pi^*-{}^5D_0$ energy gap (3100 cm^{-1}, as estimated from the 0−0 phonon transition of the $^3\pi\pi^*$ emission of **11**) is sufficient to prevent back transfer at room temperature. This strongly contrasts with the faint Eu-centered emission detected for [Eu(**L7**)$(NO_3)_3$] ($E(^3\pi\pi^*) - E(^5D_0)$ = 1980 cm^{-1}),[9] and we conclude that the replacement of π donors O(ether) in **L7** by weak π acceptors O(carboxylate) in **L11** bound to the 6 position of the benzimidazole ring increases the energy of the $^3\pi\pi^*$ level to such an extent that efficient sensitization

(29) Piguet, C.; Bünzli, J.-C. G.; Bernardinelli, G.; Hopfgartner, G.; Petoud, S.; Schaad, O. *J. Am. Chem. Soc.* **1996**, *118*, 6681 and references therein.
(30) Frey, S. T.; de Horrocks, W. W., Jr. *Inorg. Chim. Acta* **1995**, *229*, 383.

Table 5. Selected Bond Distances (Å) and Bond Angles (Degrees) for [Lu(L11)(CF_3CO_2)$_3$·H_2O] (14)

		Bond Distances			
Lu−N1	2.507(4)	Lu−N2	2.473(4)	Lu−N4	2.428(4)
Lu−O01	2.281(5)	Lu−O1a	2.437(4)	Lu−O2a	2.394(5)
Lu−O1b	2.194(4)	Lu−O1c	2.192(6)		
		Bite Angles			
N1−Lu−N2	66.0(1)	N1−Lu−N4	66.0(1)	N2−Lu−N4	131.7(1)
O1a-Lu−O2a	54.5(2)				
		N−Lu−O Angles			
N1−Lu−O1a	115.0(1)	N1−Lu−O1b	140.1(1)	N1−Lu−O1c	75.6(2)
N1−Lu−O2a	78.3(2)	N2−Lu−O1a	130.7(2)	N2−Lu−O1b	77.2(1)
N2−Lu−O1c	77.1(2)	N2−Lu−O2a	79.9(2)	N4−Lu−O1a	75.8(2)
N4−Lu−O1b	149.9(1)	N4−Lu−O1c	86.7(2)	N4−Lu−O2a	95.1(2)
		O−Lu−O Angles			
O1a−Lu−O1b	77.7(1)	O1a−Lu−O1c	152.1(2)	O1b−Lu−O1c	111.5(2)
O1b−Lu−O2a	80.7(2)	O1c−Lu−O2a	150.5(2)		

Table 6. Corrected Integrated Intensities (I_{rel}) and Main Identified Eu(^7F_j) Energy Levels (cm^{-1}, j = 1−4, Origin $^7F_0$) in [Eu(L11)(NO_3)$_3$]·2H_2O (10) As Calculated from Luminescence Spectra in the Solid State at 20 K

level	E/cm^{-1}	I_{rel}	level	E/cm^{-1}	I_{rel}
$^7F_0$ (ν_{exc})[a]	17227				
$^7F_1$	299	1.00	$^7F_4$	2529	0.94
	365			2600	
	449			2625	
$^7F_2$	966	7.33		2675	
	979			2776	
	1020			2868	
	1072			2922	
	1132				
$^7F_3$	1825	0.13			
	1873				
	1886				
	1923				

[a] Energy of the $^5D_0 \leftarrow {}^7F_0$ transition (given in cm^{-1}) used as λ_{exc} for the laser-excited emission spectra.

of Eu(III) occurs at room temperature, a crucial point for the design of luminescent lanthanide-containing materials with practical applications.[31] The Eu($^5D_0$) lifetime is similar to that obtained for hydrated [Eu(**L7**)(NO_3)$_3$] (τ = 1.14 ms at 10 K),[9] in which only interstitial water molecules reduce the emission lifetime via second sphere interactions.[32] The coordination of one water molecule to Eu(III) is expected to reduce the lifetime to ca. 0.60 ms, as reported for the analogous 10-coordinated complex [Eu(**L4**)(NO_3)$_3$·H_2O],[8] and we conclude that the water molecules in **10** do not interact with Eu(III) in the first coordination sphere. The detailed analysis of the emission spectra of **10** obtained under selective irradiation of $^5D_0 \leftarrow {}^7F_0$ or via the ligand-centered $^1\pi\pi^*$ level evidences maximum multiplicity ($2J$ + 1) for the ^7F_j (j = 1−4) levels in agreement with a low symmetry of the Eu(III) site. The considerable intensities of the hypersensitive $^5D_0 \rightarrow {}^7F_2$ transition [$I(^5D_0 \rightarrow {}^7F_2)/I(^5D_0 \rightarrow {}^7F_1)$ = 7.33; Table 6] together with the splitting pattern of the $^7F_1$ and $^7F_2$ levels are close to those observed for [Eu(**L7**)(NO_3)$_3$] for which the crystal structure indicates a C_1-symmetrical nine-coordinated environment,[9] and we can safely assign a similar coordination sphere for Eu(III) in **10**.

Although [Tb(**L7**)(NO_3)$_3$] exhibited no Tb-centered emission in the temperature range 20−295 K as a result of an efficient Tb → ligand energy back transfer,[9] [Tb(**L11**)(NO_3)$_3$]·2H_2O (**12**) displays a weak green emission at room temperature upon ligand excitation ($^1\pi\pi^*$: 26 668 cm^{-1}) or via direct excitation of the metal ($^5D_4 \leftarrow {}^7F_6$: 20 492 cm^{-1}) in line with the higher energy of the triplet state in **L11** (Figure S6, Supporting Information). Both the intensity of the Tb-centered emission bands assigned to the $^5D_4 \rightarrow {}^7F_j$ (j = 1−6) transitions and the associated lifetime of the Tb($^5D_4$) level [0.18(4) ms at 295 K to 0.95(1) ms at 20 K; Table S8, Supporting Information] significantly increase upon cooling the sample. Analysis of $\tau(^5D_4)$ in the range 77−295 K according to an Arrhenius plot of the type $\ln(\tau^{-1} - \tau_0^{-1}) = A - (E_a/RT)$ (τ_0 is the lifetime in the absence of the quenching process, taken here for τ at 20 K)[33] gives a straight line corresponding to an activation energy E_a = 203 ± 15 cm^{-1}, very similar to that found for the Tb($^5D_4$) → $^3\pi\pi^*$ energy back transfer in [Tb(**L4**)(NO_3)$_3$], 200 ± 50 cm^{-1}, for which the terdentate-centered $^3\pi\pi^*$ level lies at 21 800 cm^{-1}.[9] Upon irradiation via the ligand-centered $^1\pi\pi^*$ excited state (λ_{exc} = 32 468 cm^{-1}), a broad faint emission covering the 25 000−15 400 cm^{-1} domain reminiscent of the emission of the $^3\pi\pi^*$ level observed for the Gd complex **11** superimposes with the terbium-centered emission. Its associated lifetime [0.28(1) ms at 20 K] is comparable to that found for the decay of the $^3\pi\pi^*$ level in **11** (0.75 ms), which strongly supports the proposed back transfer process as the main quenching mechanism of the Tb-centered emission in **12**.

Conclusions

The rational variation of the global anisometry of the receptors **L11**−**L13** associated with (i) the specific connection of semirigid lipophilic side arms at the 5 or 6 position of the benzimidazole rings and (ii) the trans−trans → cis−cis conformational change of the terdentate unit occurring upon complexation demonstrates that extended semirigid side arms connected by poorly flexible carboxylate spacers are compatible with addressable mesomorphism as previously established for less rigid and shorter analogues **L4**, **L5**, and **L7** pos-

(31) (a) Deng, H.; Gin, D. L.; Smith, R. C. *J. Am. Chem. Soc.* **1998**, *120*, 3522. (b) Weder, C.; Sarwa, C.; Montali, A.; Bastiaansen, C.; Smith, P. *Science* **1998**, *279*, 835. (c) Binnemans, K.; Van Deun, R.; Görller-Walrand, C.; Collinson, S. R.; Martin, F.; Bruce, D. W.; Wickleder, C. *Phys. Chem. Chem. Phys.* **2000**, *2*, 3753.

(32) Beeby, A.; Clarkson, I. M.; Dickins, R. S.; Faulkner, S.; Parker, D.; Royle, L.; de Sousa, A. S.; Williams, J. A. G.; Woods, M. *J. Chem. Soc., Perkin Trans. 2* **1999**, 493.

(33) Charbonnière, L. J.; Balsiger, C.; Schenk, K. J.; Bünzli, J.-C. G. *J. Chem. Soc., Dalton Trans.* **1998**, 505.

sessing ether spacers.[8,9] Moreover, the introduction of carboxylate spacers between the aromatic rings induces stereoelectronic constraints which provide crossed arrangements of successive aromatic groups (interplanar angles 45−85°), thus leading to nonplanar arrangement of the extended aromatic cores in **L11**−**L13**. However, the crystal structures of **L12b** and [Lu(**L11**)$(CF_3CO_2)_3$·H_2O] suggest that these considerable intramolecular distortions do not prevent efficient intermolecular π-stacking interactions which are invoked for rationalizing (i) the parallel arrangement of terdentate receptors in the crystal of **L12b**, (ii) the excimer emission of **L11** in the solid state, and (iii) the stabilization of the Col_R mesophase. According to an electronic point of view, the weakly π-accepting carboxylate spacers connecting the benzimidazole and the phenyl rings act as insulators, providing specific photophysical properties associated with either the terdentate binding unit or the polyaromatic side arms. The higher energies of the ligand-centered $^1\pi\pi^*$ and $^3\pi\pi^*$ levels in **L11** and **L12** compared to those in **L5** and **L7** are the logical consequences of the electrowithdrawing character of the spacers, a crucial point for inducing room-temperature Eu-centered red emission in the complex [Eu(**L11**)$(NO_3)_3$]·$2H_2O$ (**10**), which contrasts with the nonluminescent analogue [Eu(**L7**)$(NO_3)_3$].[9] Finally, the systematic extension of the semirigid aromatic side arms when going from **L4**−**L7** (one phenyl ring) to **L11** and **L12** (two phenyl rings) and **L13** (three phenyl rings) increases the melting and clearing temperatures of the ligands and of their complexes in line with the existence of stronger intermolecular interactions in the solid state and in the mesophases resulting from the increasing axial anisometries of the receptors (**L4**−**L7** < **L11**, **L12** < **L13**). The latter ratio is also crucial for controlling columnar vs smectogenic behavior,[34] and the Col_R mesophase detected for **L11** strongly supports the concept of Diele and co-workers,[13,14] who propose that minimal overlap between the terminal rigid cores in bent molecules is required to induce columnar mesomorphism for V-shaped molecules. This approach offers a fascinating opportunity for introducing bent terdentate binding units into mesophases because liquid-crystalline behavior is thus not restricted to rodlike receptors. However, the lack of mesomorphism of the lanthanide complexes highlights the importance of the spatial expansion brought by the metallic cores in metallomesogens.

Experimental Section

Solvents and starting materials were purchased from Fluka AG (Buchs, Switzerland) and used without further purification, unless otherwise stated. Acetonitrile, dichloromethane, *N*,*N*-dimethylformamide (DMF), dimethyl sulfoxide (DMSO), and triethylamine were distilled from CaH_2, tetrahydrofuran (THF) was distilled from sodium, and thionyl chloride was distilled from elemental sulfur. 2,6-Bis(1-ethyl-6-hydroxybenzimidazol-2-yl)pyridine (**7**)[9] and 2,6-bis(1-ethyl-5-hydroxybenzimidazol-2-yl)pyridine (**8**)[8] were obtained according to literature procedures. The nitrate $Ln(NO_3)_3$·nH_2O (Ln = La to Lu) and trifluoroacetate $Lu(CF_3CO_2)_3$·H_2O salts were prepared from the corresponding oxides (Rhodia; 99.99%) according to literature procedures.[35] The Ln content of solutions and solid salts was determined by complexometric titrations with Titriplex III (Merck) in the presence of urotropine and xylene orange.[36] Silica gel (Merck 60; 0.040−0.060 mm) was used for preparative column chromatography.

Preparation of Benzyl 4-[[4-(Dodecyloxy)benzoyl]oxy]-benzoate (3). 4-(Dodecyloxy)benzoic acid (**1**; 3.06 g, 10 mmol), benzyl 4-hydroxybenzoate (**2**; 2.28 g, 10 mmol), *N*,*N*′-dicyclohexylcarbodiimide (DCC; 2.06 g, 10 mmol), and 4-(dimethylamino)pyridine (DMAP; 1.22 g, 10 mmol) were refluxed in dichloromethane (250 mL) for 48 h under an inert atmosphere. The resulting mixture was filtered, and the solvent was evaporated to dryness. The crude residue was purified by column chromatography (silica gel; CH_2Cl_2) and then crystallized from hot ethanol to give 4.88 g (9.4 mmol, yield 94%) of **3** as white microcrystals. mp: 62 °C. ^{1}H NMR ($CDCl_3$): δ 0.85 (3 H, t, $J^3 = 7$ Hz), 1.23 (18 H, m), 1.78 (2 H, m), 4.01 (2 H, t, $J^3 = 7$ Hz), 5.34 (2 H, s), 6.94 (2 H, d, $J^3 = 9$ Hz), 7.26 (2 H, d, $J^3 = 9$ Hz), 7.26−7.42 (5 H, m), 8.10 (2 H, d, $J^3 = 9$ Hz), 8.12 (2 H, d, $J^3 = 9$ Hz). EI-MS: *m*/*z* 516 (M^+). The same procedure was used with **1b** to give 93% of **3b**. Mp: 56−58 °C. ^{1}H NMR ($CDCl_3$): δ 0.88 (3 H, t, $J^3 = 7$ Hz), 1.32 (6 H, m), 1.78 (2 H, m), 4.01 (2 H, t, $J^3 = 7$ Hz), 5.34 (2 H, s), 6.94 (2 H, d, $J^3 = 9$ Hz), 7.26 (2 H, d, $J^3 = 9$ Hz), 7.26−7.42 (5 H, m), 8.10 (2 H, d, $J^3 = 9$ Hz), 8.12 (2 H, d, $J^3 = 9$ Hz). EI-MS: *m*/*z* 432 (M^+).

Preparation of 4-[[4-(Dodecyloxy)benzoyl]oxy]benzoic Acid (4). 3 (4.0 g, 7.74 mmol) was dissolved in ethyl acetate (250 mL) containing a suspension of a Pd/C catalyst (10% Pd/C, 40 mg). After the mixture was stirred for 24 h under a hydrogen atmosphere (1 atm), the solvent was evaporated and the residue dissolved in THF (50 mL). The catalyst was removed by filtration and the filtrate crystallized with the addition of ethyl acetate to give 2.77 g (6.5 mmol, yield 84%) of **4** as white microcrystals. mp: 112−115 °C. ^{1}H NMR ($CDCl_3$): δ 0.84 (3 H, t, $J^3 = 7$ Hz), 1.23 (18 H, m), 1.78 (2 H, m), 4.01 (2 H, t, $J^3 = 7$ Hz), 6.95 (2 H, d, $J^3 = 9$ Hz), 7.30 (2 H, d, $J^3 = 9$ Hz), 8.10 (2 H, d, $J^3 = 9$ Hz), 8.16 (2 H, d, $J^3 = 9$ Hz). EI-MS: *m*/*z* 426 ($[M]^+$). ESI-MS (CH_2Cl_2): *m*/*z* 425.2 ($[M - H]^-$). The same procedure was used with **3b** to give 89% of **4b**. Mp: 160−162 °C. ^{1}H NMR ($CDCl_3$): δ 0.88 (3 H, t, $J^3 = 7$ Hz), 1.31 (6 H, m), 1.78 (2 H, m), 4.01 (2 H, t, $J^3 = 7$ Hz), 6.95 (2 H, d, $J^3 = 9$ Hz), 7.30 (2 H, d, $J^3 = 9$ Hz), 8.10 (2 H, d, $J^3 = 9$ Hz), 8.16 (2 H, d, $J^3 = 9$ Hz). ESI-MS (CH_2Cl_2): molecular peak not detected.

Preparation of Benzyl 4-[[4-[[4-(Dodecyloxy)benzoyl]-oxy]benzoyl]oxy]benzoate (5). 4 and **2** were reacted in the same conditions as those described for the preparation of **3** to give 80% of **5** as white microcrystals. mp: 109−111 °C. ^{1}H NMR ($CDCl_3$): δ 0.84 (3 H, t, $J^3 = 7$ Hz), 1.23 (18 H, m), 1.79 (2 H, m), 4.02 (2 H, t, $J^3 = 7$ Hz), 5.34 (2 H, s), 6.96 (2 H, d, $J^3 = 9$ Hz), 7.23−7.43 (9 H, m), 8.10−8.20 (4 H, m), 8.26 (2 H, d, $J^3 = 9$ Hz). EI-MS: *m*/*z* 409 ($[M - C_{14}H_{11}O_3]^+$), 289 ($[M - C_{21}H_{15}O_5]^+$).

Preparation of 4-[[4-[[4-(Dodecyloxy)benzoyl]oxy]benzoyl]oxy]benzoic Acid (6). The same procedure as that described for the preparation of **4** was applied to **5** to give 82% of **6**, which was crystallized from hot ethanol. mp: 171−173 °C. ^{1}H NMR ($CDCl_3$): δ 0.84 (3 H, t, $J^3 = 7$ Hz), 1.23 (18 H, m), 1.79 (2 H, m), 4.02 (2 H, t, $J^3 = 7$ Hz), 6.96 (2 H, d, $J^3 = 9$ Hz), 7.33 (2 H, d, $J^3 = 9$ Hz), 7.36 (2 H, d, $J^3 = 9$ Hz), 8.12 (2 H, d, $J^3 = 9$ Hz), 8.17 (2 H, d, $J^3 = 9$ Hz), 8.25 (2 H, d, $J^3 = 9$ Hz). ESI-MS (CH_2Cl_2): *m*/*z* 545.2 ($[M - H]^-$).

Preparation of the Ligands L11, L12, L12b, and L13. **4** (1.096 g, 2.57 mmol), **7** (0.512 g, 1.28 mmol), DCC (0.529 g, 2.57 mmol), and DMAP (64 mg, 0.52 mmol) were refluxed in dichloromethane (250 mL) for 48 h under an inert atmosphere. The resulting solution was washed with half-saturated aqueous NaCl (100 mL), and the organic phase was separated. The aqueous phase was extracted with dichloromethane (3 × 50

(34) Bruce, D. W. *Acc. Chem. Res.* **2000**, *33*, 831 and references therein.

(35) Desreux, J. F. In *Lanthanide Probes in Life, Chemical and Earth Sciences*; Bünzli, J.-C. G., Choppin, G. R., Eds.; Elsevier Publishing Co.: Amsterdam, The Netherlands, 1989; Chapter 2.

(36) Schwarzenbach, G. *Complexometric Titrations*; Chapman & Hall: London, 1957; pp 8ff.

mL), the combined organic phases were dried (Na_2SO_4), and the solvent was evaporated. The crude residue was purified by column chromatography (silica gel; CH_2Cl_2/MeOH, 100:0 → 99:1) and crystallized twice from propionitrile to give 1.243 g (1.02 mmol, yield 81%) of **L11** as a white microcrystalline powder. The same procedure was used to obtain **L12** (yield 81%) from **4** and **8**, **L12b** (yield 82%) from **4b** and **8**, and **L13** (yield 78%) from **6** and **8**.

L11. mp: 195 °C. Isotropization: 203 °C. ^{1}H NMR ($CDCl_3$): δ 0.84 (6 H, t, $J^3 = 7$ Hz, CH_3−$C_{11}H_{22}$O), 1.23 (36 H, m, CH_3−C_9H_{18}−C_2H_4O), 1.38 (6 H, t, $J^3 = 7$ Hz, CH_3−CH_2−N), 1.79 (4 H, m, $C_{10}H_{21}$−CH_2−CH_2O), 4.02 (4 H, t, $J^3 = 7$ Hz, $C_{11}H_{23}$−CH_2O), 4.78 (4 H, q, $J^3 = 7$ Hz, CH_3−CH_2−N), 6.96 (4 H, d, $J^3 = 9$ Hz, H^{phenyl}), 7.22 (2 H, dd, $J^3 = 9$ Hz, $J^4 = 2$ Hz, H^{benzim}), 7.36 (4 H, d, $J^3 = 9$ Hz, H^{phenyl}), 7.37 (2 H, d, $J^4 = 2$ Hz, H^{benzim}), 7.87 (2 H, d, $J^3 = 9$ Hz, H^{benzim}), 8.05 (1 H, t, $J^3 = 8$ Hz, H^{py}), 8.12 (4 H, d, $J^3 = 9$ Hz, H^{phenyl}), 8.30 (4 H, d, $J^3 = 9$ Hz, H^{phenyl}), 8.33 (2 H, d, $J^3 = 8$ Hz, H^{py}). ^{13}C NMR ($CDCl_3$): δ 14.35, 15.63 (primary C); 22.90, 26.18, 29.28, 29.56, 29.76, 29.79, 29.84, 29.87, 32.12, 40.29, 68.59 (secondary C); 103.90, 114.62, 121.08, 122.38, 127.06, 132.06, 132.64, 136.33 (tertiary C); 117.52, 125.94, 138.49, 140.97, 147.64, 149.95, 150.90, 155.54, 164.04, 164.58, 165.17 (quaternary C). ESI-MS (CH_2Cl_2): m/z 1216.9 ($[M + H]^+$). Anal. Calcd for $C_{75}H_{85}N_5O_{10}$: C, 74.05; N, 5.76; H, 7.04. Found: C, 74.00; N, 5.76; H, 7.02.

L12. mp: 206 °C. Isotropization: 322 °C. ^{1}H NMR ($CDCl_3$): δ 0.84 (6 H, t, $J^3 = 7$ Hz, CH_3−$C_{11}H_{22}$O), 1.23 (36 H, m, CH_3−C_9H_{18}−C_2H_4O), 1.38 (6 H, t, $J^3 = 7$ Hz, CH_3−CH_2−N), 1.79 (4 H, m, $C_{10}H_{21}$−CH_2−CH_2O), 4.02 (4 H, t, $J^3 = 7$ Hz, $C_{11}H_{23}$−CH_2O), 4.78 (4 H, q, $J^3 = 7$ Hz, CH_3−CH_2−N), 6.96 (4 H, d, $J^3 = 9$ Hz, H^{phenyl}), 7.22 (2 H, dd, $J^3 = 9$ Hz, $J^4 = 2$ Hz, H^{benzim}), 7.36 (4 H, d, $J^3 = 9$ Hz, H^{phenyl}), 7.50 (2 H, d, $J^3 = 9$ Hz, H^{benzim}), 7.67 (2 H, d, $J^4 = 2$ Hz, H^{benzim}), 8.06 (1 H, t, $J^3 = 8$ Hz, H^{py}), 8.13 (4 H, d, $J^3 = 9$ Hz, H^{phenyl}), 8.32 (4 H, d, $J^3 = 9$ Hz, H^{phenyl}), 8.34 (2 H, d, $J^3 = 8$ Hz, H^{py}). ^{13}C NMR ($CDCl_3$): δ 14.34, 15.69 (primary C); 22.90, 26.18, 29.28, 29.56, 29.76, 29.79, 29.84, 29.86, 32.12, 40.31, 68.59 (secondary C); 110.82, 113.14, 114.61, 118.50, 122.32, 127.17, 132.10, 132.63, 138.59 (tertiary C); 121.14, 122.16, 126.30, 134.08, 143.03, 147.16, 149.80, 150.92, 155.57, 164.02, 164.57, 165.27 (quaternary C). ESI-MS (CH_2Cl_2): m/z 1216.9 ($[M + H]^+$). Anal. Calcd for $C_{75}H_{85}N_5O_{10}$: C, 74.05; N, 5.76; H, 7.04. Found: C, 74.01; N, 5.76; H, 7.04.

L12b. mp: 187 °C. Isotropization: >320 °C. ^{1}H NMR ($CDCl_3$): δ 0.89 (6 H, t, $J^3 = 7$ Hz, CH_3−C_5H_{10}O), 1.33 (12 H, m, CH_3−C_3H_6−C_2H_4O), 1.39 (6 H, t, $J^3 = 7$ Hz, CH_3−CH_2−N), 1.80 (4 H, m, C_4H_9−CH_2−CH_2O), 4.02 (4 H, t, $J^3 = 7$ Hz, C_5H_{11}−CH_2O), 4.79 (4 H, q, $J^3 = 7$ Hz, CH_3−CH_2−N), 6.96 (4 H, d, $J^3 = 9$ Hz, H^{phenyl}), 7.24 (2 H, dd, $J^3 = 9$ Hz, $J^4 = 2$ Hz, H^{benzim}), 7.36 (4 H, d, $J^3 = 9$ Hz, H^{phenyl}), 7.50 (2 H, d, $J^3 = 9$ Hz, H^{benzim}), 7.71 (2 H, d, $J^4 = 2$ Hz, H^{benzim}), 8.06 (1 H, t, $J^3 = 8$ Hz, H^{py}), 8.13 (4 H, d, $J^3 = 9$ Hz, H^{phenyl}), 8.32 (4 H, d, $J^3 = 9$ Hz, H^{phenyl}), 8.38 (2 H, d, $J^3 = 8$ Hz, H^{py}). ^{13}C NMR ($CDCl_3$): δ 14.24, 15.69 (primary C); 22.80, 25.86, 29.25, 31.74, 40.44, 68.58 (secondary C); 110.95, 112.99, 114.61, 122.34 132.11, 132.64 (tertiary C); 121.13, 127.08, 134.08, 143.03, 147.16, 149.80, 150.92, 155.61, 164.02, 164.57, 165.22 (quaternary C). ESI-MS (CH_2Cl_2): m/z 1048.4 ($[M + H]^+$). Anal. Calcd for $C_{63}H_{61}N_5O_{10}$: C, 72.19; N, 6.68; H, 5.87. Found: C, 71.55; N, 6.55; H, 5.98.

L13. mp: 220 °C. Isotropization: >320 °C. ^{1}H NMR ($CDCl_3$): δ 0.85 (6 H, t, $J^3 = 7$ Hz, CH_3−$C_{11}H_{22}$O), 1.23 (36 H, m, CH_3−C_9H_{18}−C_2H_4O), 1.38 (6 H, t, $J^3 = 7$ Hz, CH_3−CH_2−N), 1.80 (4 H, m, $C_{10}H_{21}$−CH_2−CH_2O), 4.02 (4 H, t, $J^3 = 7$ Hz, $C_{11}H_{23}$−CH_2O), 4.79 (4 H, q, $J^3 = 7$ Hz, CH_3-CH_2−N), 6.96 (4 H, d, $J^3 = 9$ Hz, H^{phenyl}), 7.22 (2 H, dd, $J^3 = 9$ Hz, $J^4 = 2$ Hz, H^{benzim}), 7.36 (4 H, d, $J^3 = 9$ Hz, H^{phenyl}), 7.39 (4 H, d, $J^3 = 9$ Hz, H^{phenyl}), 7.50 (2 H, d, $J^3 = 9$ Hz, H^{benzim}), 7.67 (2 H, d, $J^4 = 2$ Hz, H^{benzim}), 8.05 (1 H, t, $J^3 = 8$ Hz, H^{py}), 8.13 (4 H, d, $J^3 = 9$ Hz, H^{phenyl}), 8.27 (4 H, d, $J^3 = 9$ Hz, H^{phenyl}), 8.33 (4 H, d, $J^3 = 9$ Hz, H^{phenyl}), 8.34 (2 H, d, $J^3 = 8$ Hz, H^{py}). ^{13}C NMR ($CDCl_3$): δ 14.34, 15.71 (primary C); 22.90, 26.18, 29.28, 29.56, 29.76, 29.79, 29.84, 29.86, 32.12, 40.26, 68.60 (secondary C); 110.76, 113.22, 114.63, 118.32, 122.24, 122.39, 126.17, 132.14, 132.17, 138.49 (tertiary C); 121.05, 125.56, 127.52, 134.22, 143.36, 147.03, 149.99, 151.10, 155.29, 155.85, 164.07, 164.19, 164.51, 165.22 (quaternary C). ESI-MS (CH_2Cl_2): m/z 1457.6 ($[M + H]^+$). Anal. Calcd for $C_{89}H_{93}N_5O_{14}$: C, 73.38; N, 4.81; H, 6.43. Found: C, 73.13; N, 4.74; H, 6.40.

Preparation of [Ln(L11)(NO$_3$)$_3$]·xH$_2$O (9−13) and [Lu(L11)(CF$_3$CO$_2$)$_3$·H$_2$O] (14). **L11** (0.053 mmol) in dichloromethane (5 mL) was added to $Ln(NO_3)_3$·$x$$H_2O$ ($x = 2-6$, 0.053 mmol) or $Lu(CF_3CO_2)_3$·H_2O (0.053 mmol) in acetonitrile (5 mL). After 1 h of stirring at room temperature, the solvents were evaporated to dryness and the residual solid was solubilized in hot propionitrile or butyronitrile. Cooling the solution produced 74−85% of complexes [Ln(**L11**)$(NO_3)_3$]·$x$$H_2O$ (Ln = La, $x = 0$, **9**; Ln = Eu, $x = 2$, **10**; Ln = Gd, $x = 1$, **11**; Ln = Tb, $x = 2$, **12**; Ln = Lu, $x = 1$, **13**) and [Lu(**L11**)$(CF_3CO_2)_3$·H_2O] (**14**) as white microcrystalline powders after drying under vacuum. X-ray quality crystals of **14** were obtained with the same procedure, but the crystals were directly transferred from the mother liquor to the diffractometer. Complexes **9**−**14** were characterized by their IR spectra and gave satisfactory elemental analyses (Table S9, Supporting Information).

Physicochemical Measurements. Reflectance spectra were recorded as finely ground powders dispersed in MgO (5%), with MgO as the reference, on a Perkin-Elmer Lambda 900 spectrophotometer equipped with a PELA-1000 integration sphere from Labsphere. Electronic spectra in the UV−visible range were recorded at 20 °C from 10^{-3}−10^{-5} M CH_3CN/CH_2Cl_2 (7:3) solutions for solubility reasons with a Perkin-Elmer Lambda 900 spectrometer using quartz cells of 0.1 and 1 cm path lengths. IR spectra were obtained from KBr pellets with a Perkin-Elmer 883 spectrometer. ^{1}H and ^{13}C NMR spectra were recorded at 25 °C on a broad-band Varian Gemini 300 spectrometer. Chemical shifts are given in ppm with respect to TMS. EI-MS (70 eV) were recorded with VG-7000E and Finnigan-4000 instruments. Pneumatically assisted electrospray (ES-MS) mass spectra were recorded from CH_2Cl_2 solutions on a Finnigan MAT SSQ 7000. The experimental procedures for high-resolution, laser-excited luminescence measurements were published previously.[24] Solid-state samples were finely powdered, and low temperature (295−20 K) was achieved by means of a Cryodyne model 22 closed-cycle refrigerator from CTI Cryogenics. Luminescence spectra were corrected for the instrumental function, but not excitation spectra. Lifetimes are averages of at least three to five independent determinations. Ligand excitation and emission spectra were recorded on a Perkin-Elmer LS-50B spectrometer equipped for low-temperature measurements. DSC traces were obtained with a Seiko DSC 220C differential scanning calorimeter from 3−5 mg samples (5−10 °C·min^{-1}, under N_2). Thermogravimetric analyses were performed with a Seiko TG/DTA 320 thermogravimetric balance (under N_2). The characterization of the mesophases was performed with a Leitz Orthoplan-Pol polarizing microscope with a Leitz LL 20 × 0.40 polarizing objective and equipped with a Linkam THMS 600 variable-temperature stage. The XRD patterns were obtained with two different experimental setups, and in all cases, the crude powder was filled in Lindemann capillaries of 1 mm diameter. The characterization of the wide-angle region and the measurements of the periodicities was achieved using a linear monochromatic Cu Kα_1 beam obtained with a sealed-tube generator (900 W) and a bent quartz monochromator. One set of diffraction patterns was registered with a curved counter Inel CPS 120, for which the sample temperature was controlled within ±0.05 °C; periodicities up to 60 Å could be measured. The other set of diffraction patterns was registered on an Image Plate; the cell parameters were calculated from the position of the reflection at the smallest Bragg angle, which was in all cases the most intense. Periodicities up to 90 Å could be measured, and the sample temperature was controlled within ±0.3 °C. The exposure times were varied from 1 to 24 h depending on the specific reflections being sought (with weaker reflections obviously taking longer exposure times). Elemental analyses were performed by Dr. H. Eder from the Microchemical Laboratory of the University of Geneva.

Computational Details. In this work, all of the AM1 geometry optimizations and ZINDO UV−visible spectra calculations were performed using the respective modules of the

Table 7. Summary of Crystal Data, Intensity Measurements, and Structure Refinement for L12b and [Lu(L11)(CF$_3$CO$_2$)$_3$·H$_2$O] (14)

	L12b	14
formula	$C_{63}H_{61}N_5O_{10}$	$LuC_{81}H_{87}N_5O_{17}F_9$
mol wt	1048.3	1748.7
color	colorless	colorless
cryst syst	triclinic	triclinic
space group	$P\bar{1}$	$P\bar{1}$
a, Å	9.7295(6)	13.6773(11)
b, Å	13.7023(10)	14.6177(11)
c, Å	20.9998(14)	20.809(2)
α, deg	102.886(8)	75.803(11)
β, deg	99.294(7)	79.667(11)
γ, deg	90.223(8)	89.016(10)
V, Å^3	2691.0(3)	3966.3(6)
Z	2	2
d_{calc}, g·cm^{-3}	1.294	1.464
$\mu_{Mo\,K\alpha}$, mm^{-1}	0.09	1.34
T_{min}/T_{max}	0.9718/0.9935	0.7843/0.9517
cryst size, mm	0.08 × 0.26 × 0.29	0.037 × 0.11 × 0.30
temp, K	200	200
reflcns measd	21 466	39 110
θ range	4.4° < 2θ < 51.9°	3.9° < 2θ < 51.8°
reflcns unique	9820	14 357
reflcns obsd ($\|F_o\| > 4\sigma(F_o)$)	5287	9083
variables	752	1051
GOF	2.02(2)	0.989(1)
w	$1/(\sigma^2F_o + 0.0002F_o^2)$	$1/(\sigma^2F_o + 0.0003F_o^2)$
R	0.053	0.041
R_w	0.056	0.040

Cerius2 Quantum Mechanics Workbench.[37] A Silicon graphics O2 workstation was used to do all of the computations.

X-ray Crystal Structure Determination of L12b. A summary of the crystal data, intensity measurements, and structure refinements is reported in Table 7.

Data Collection and Processing. Stoe IPDS diffractometer, $\Delta\varphi$/image 1.0°, $\varphi_{min,max} = 0-200°$, irradiation time/image 5 min, Mo Kα radiation ($\lambda = 0.7107$ Å).

Structure Analysis and Refinement. Data were corrected for Lorentz, polarization, and absorption effects.[38] The structure was solved by direct methods using MULTAN 87[39] and full-matrix least-squares refinements (on F). All other calculations used a XTAL[40] system and ORTEP II[41] programs. The non-H atoms were refined with anisotropic displacement parameters except C58. H atoms were placed in calculated positions and contributed to F_c. One of the aliphatic chains (C54−C59) was disordered and refined with two atomic sites for each carbon atom (population parameters = 0.5) with restraints on bond distances and bond angles.

X-ray Crystal Structure Determination of 14. A summary of the crystal data, intensity measurements, and structure refinements is reported in Table 7.

Data Collection and Processing. Stoe IPDS diffractometer, $\Delta\varphi$/image 1.0°, $\varphi_{min,max} = 0-250°$, irradiation time/image 6 min, Mo Kα radiation ($\lambda = 0.7107$ Å).

Structure Analysis and Refinement. The same procedure as that described for **L12b** was used for **14**. The non-H atoms were refined with anisotropic displacement parameters. The H atoms were placed in calculated positions and contributed to F_c calculations except for the two hydrogen atoms of the water molecules, which were observed and refined with $U_{iso} = 0.05$. The fluorine atoms of the trifluoroacetate anion c were disordered and refined with restraints on C−F bond distances and C−C−F and F−C−F bond angles.

Acknowledgment. We gratefully acknowledge H. Lartigue, V. Foiret, and X. Melich for their technical assistance. J.-C.G.B. thanks the Fondation Herbette (Lausanne) for the gift of spectroscopic equipment. This work is supported through Grant 4047-057479 from the Swiss National Science Foundation, National Research Program 47 “Supramolecular Functional Materials”.

Supporting Information Available: Tables of bond distances, bond angles, and selected least-squares planes data for **L12b** (Tables S1 and S2) and **14** (Table S7), tables of selected computed energy levels and orbitals obtained by ZINDO for **L11** and **L12** (Tables S3−S6), table of lifetime data for **10** and **12** (Table S8), and table of elemental analyses for the complexes **9**−**14** (Table S9). Figure S1 shows a Walsh diagram of frontier orbitals calculated by ZINDO for **L11** and **L12**. Figure S2 shows the packing in the unit cell of **14**. Figure S3 shows the texture of the Col$_R$ mesophase of **L11**. Figures S4−S6 show selected emission and excitation spectra of **10** and **12** recorded under various conditions (PDF). This material is available free of charge via the Internet at http://pubs.acs.org.

(37) Cerius^2 4.0, Software Environment for Chemical Computing, Molecular Simulations Inc., 9685 Scranton Road, San Diego, CA 92121-3752.

(38) Stoe & Cie. *X.-RED*, version 1.14; Stoe & Cie: Darmstadt, Germany, 1999.

(39) Main, P.; Fiske, S. J.; Hull, S. E.; Lessinger, L.; Germain, D.; Declercq, J. P.; Woolfson, M. M. *MULTAN 87*; University of York: York, U.K., 1987.

(40) Hall, S. R., Flack, H. D., Stewart, J. M., Eds. *XTAL 3.2 User's Manual*; University of Maryland: College Park, MD, 1992.

(41) Johnson, C. K. *ORTEP II*; Report ORNL-5138; Oak Ridge National Laboratory: Oak Ridge, TN, 1976.